

Submitted to ApJ

Stability of the Accretion Flows with Stalled Shocks in Core-Collapse Supernovae

Tatsuya Yamasaki¹ and Shoichi Yamada^{2,3}

ABSTRACT

Bearing in mind the application to the theory of core-collapse supernovae, we performed a global linear analysis on the stability of spherically symmetric accretion flows through a standing shock wave onto a proto neutron star. Both radial and non-radial modes were studied in detail. As unperturbed flows, we adopted the spherically symmetric steady solutions to the Euler equations, which were obtained in the previous paper with realistic equation of state and formulae for neutrino reaction rates taken into account. These solutions are characterized by the mass accretion rate and neutrino luminosity that are assumed to be constant in time. Then we solved the equations for linear perturbations numerically, imposing appropriate boundary conditions and obtained the eigen frequencies and eigen functions for various radial and non-radial modes. We found (1) the flows are stable for all modes if the neutrino luminosity is lower than a certain value, e.g. $\sim 1 \times 10^{52}$ ergs/s for $\dot{M} = 1.0M_{\odot}/\text{s}$. (2) For larger luminosities, the non-radial instabilities are induced, probably via the advection-acoustic cycles. Interestingly, the modes with $\ell = 2$ and 3 become unstable at first for relatively low neutrino luminosities, e.g. $\gtrsim 2 - 3 \times 10^{52}$ ergs/s for the same accretion rate, whereas the $\ell = 1$ mode is the most unstable for higher luminosities, $\sim 3 - 7 \times 10^{52}$ ergs/s. Here ℓ stands for the azimuthal index of the spherical harmonic functions, Y_{ℓ}^m . These are all oscillatory modes. (3) For still larger luminosities, $\sim 7 \times 10^{52}$ ergs/s for $\dot{M} = 1.0M_{\odot}/\text{s}$, non-oscillatory modes, both radial and non-radial, become unstable. These non-radial modes were identified

¹Yukawa Institute for Theoretical Physics, Kyoto University, Oiwake-cho, Sakyo, Kyoto 606-8502, Japan;
ytatsuya@yukawa.kyoto-u.ac.jp

²Science and Engineering, Waseda University, 3-4-1 Okubo, Shinjuku, Tokyo 169-8555, Japan;
shoichi@heap.phys.waseda.ac.jp

³Advanced Research Institute for Science and Engineering, Waseda University, 3-4-1 Okubo, Shinjuku, Tokyo 169-8555, Japan

as convection. The growth rates of the convective modes change gradually with ℓ and have a peak at $\ell = 5 - 11$, depending on the luminosity. The luminosity, at which each convective mode becomes unstable, decreases with ℓ up to $\ell = 6$ and then increases for the same accretion rate. We confirmed the results obtained by numerical simulations that the instabilities induced by the advection-acoustic cycles are more important than the convection for lower neutrino luminosities. We also modified the criterion for the convection in the presence of advection previously discussed by other authors. Furthermore, we investigated the sensitivity of the results to the inner boundary conditions and found that the nature of the instabilities is not changed qualitatively.

Subject headings: hydrodynamics — shock waves — instabilities — supernovae: general

1. Introduction

The explosion mechanism of core-collapse supernova is still remaining to be revealed. Several observations suggest that the supernova explosion is asymmetric in general. For example, the HST images of supernova 1987A, the most thoroughly investigated supernova so far, shows clear global asymmetry of the ejecta. The radiations scattered by the supernova ejecta commonly have one percent level of linear polarization, the fact naturally explained by the asymmetry of the scattering surface (Leonard et al. 2000; Wang et al. 2002). Furthermore, it is now well known that young pulsars have a large peculiar velocity (Lyne & Lorimer 1994), which is supposed to be gained by a nascent neutron star at its birth owing to the asymmetry of dynamics. On the theoretical side, the possible roles of the asymmetry in the explosion mechanism are being explored from various points of view at the moment (Kotake et al. 2006).

As a result of many multi-dimensional studies, it is now believed that the dynamics of supernova core is intrinsically asymmetric even though extrinsic factors like the rotation or magnetic field of progenitor is absent. The asymmetry is thought to be produced by some hydrodynamical instabilities, the most well known of which is convections. A couple of recent numerical simulations demonstrates, on the other hand, that another instability plays an important role in the accretion flows through the standing shock onto the proto neutron star (Blondin et al. 2003; Scheck et al. 2004; Blondin & Mezzacappa 2006; Ohnishi et al. 2006). The remarkable feature of this instability is the dominance of the $\ell = 1$ mode, where ℓ stands for the azimuthal index of the spherical harmonic functions, Y_ℓ^m . The so-called standing accretion shock instability or SASI is thus expected to be a natural explanation for

the large kick velocities of young pulsars.

The mechanism of SASI is still controversial. One of the promising mechanisms is the amplified cycle of the inward advects of vortex and entropy fluctuations and outward propagations of acoustic perturbations, which was originally discussed in the context of black hole accretions (Foglizzo & Tagger 2000; Foglizzo 2001, 2002). The mechanism was also known in the engineering field (see Howe (1975) and references therein). Most recently, however, Blondin & Mezzacappa (2006) claimed, based on their 2D numerical simulations with a simplified cooling taken into account, that the instability is induced by the purely acoustic cycles. On the other hand, Ohnishi et al. (2006) obtained the results that appear to support the advection-acoustic cycle in their 2D numerical models with more realistic heating and cooling processes taken into consideration. Obviously, more detailed linear analyses for appropriate background models and boundary conditions are needed to clarify the nature of the instabilities and that is the main purpose of this paper, in which we accomplished global linear analyses for the spherically symmetric steady accretion flows that are supposed to represent the post-bounce supernova core reasonably well. It should be emphasized that SASI is a non-local instability.

As mentioned above, the convection has been numerically explored by many researchers for the past decades. If the neutrino luminosity is larger than a certain value, there appears a so-called heating region in the post-shock flows, where the net neutrino heating occurs (Yamasaki & Yamada 2006). In this region, the entropy gradient is negative and the flow is convectively unstable if the conventional criterion for convection is applied. Recently, Foglizzo et al. (2005) demonstrated by linear analysis that the advection tends to suppress the convection. In fact, the condition for the instability is tightened and the growth rate is lowered in general. In this paper, SASI was not discussed. We think, however, the SASI and convection should be treated simultaneously and on an equal basis. It is also noted that it is important to employ a realistic equation of state and neutrino heating/cooling rates, since not only the evolution of perturbations but also the unperturbed background structure is dictated by them. In fact, the stability strongly depends on the latter. For example, the radial distributions of sound velocity or inflow velocity are crucially important for the advection-acoustic cycle. The growth rate and stability criterion for convection, on the other hand, depend not only on the entropy gradient but also on the advection time of the flow as discussed by Foglizzo et al. (2005). Moreover, the stability of accretion flows through a standing shock against radial perturbations is mainly determined by the acceleration or deceleration of the flow just behind the shock wave (Nakayama 1992, 1993, 1994). It is, hence, important to employ appropriate unperturbed background flows and boundary conditions. Some of the discrepancy mentioned above may be attributed to the difference of them.

In this paper, we accomplished global linear analyses of spherically symmetric steady accretion flows through a standing accretion shock onto a proto neutron star, using a realistic equation of state and neutrino-heating/cooling rates, and investigated the stability of the flows against both radial and non-radial perturbations. In so doing, we treated the convective instabilities and SASI on an equal basis. In the next section, we summarize the formulations, describing briefly the background steady solutions and then giving basic equations for the global linear analysis. The main results of the numerical calculations are presented in section 3. We discuss the mechanisms of instabilities found in the previous section in section 4. In section 5, we consider the dependence of the results on the assumptions we make for the inner boundary conditions and the perturbation of neutrino temperature. The final section is devoted to discussion.

2. Formulations

2.1. Unperturbed Steady Accretion Flows

The unperturbed steady background flows were obtained exactly the same way as in the previous paper (Yamasaki & Yamada 2006). The results are supposed to approximate the post-bounce accretion flows through a stalled shock wave onto a proto neutron star in the supernova core. The approximation is justified by the fact that the typical time scale for the variations of mass accretion rate and neutrino luminosity are longer than the dynamical time scale of the accretion flow. We solved the hydrodynamical equations only for the region between the shock front and the neutrino sphere, approximating the upstream flow of the shock by the free fall. We refer readers to Yamasaki & Yamada (2006) for the basic equations (Eqs. (1)-(5)) and other details, and will summarize some important elements here. The notations were also inherited from the paper.

The formulations are Newtonian. We took account of the self-gravity of the accretion flow. The neutrino transfer was not solved, since the region of interest is optically thin for neutrinos. The neutrino luminosities and spectra were assumed to be constant in time. The latter were assumed to be thermal with a temperature of 4.5MeV. The realistic equation of state by Shen et al. (1998) and the standard reaction rates for the absorptions and emissions of neutrino on free nucleons Bruenn (1988) were employed. As for the boundary conditions, we imposed the Rankine-Hugoniot relations at the shock front. At the inner boundary, on the other hand, the condition that the optical depth for neutrino be 2/3 was imposed. See Eqs. (6)-(10) and (17) in Yamasaki & Yamada (2006).

We solved these equations for a wide range of the control parameters, that is, the mass

accretion rate and neutrino luminosity. The results were shown in Figs. 2-4 in Yamasaki & Yamada (2006). It is just repeated that there is a critical luminosity for each given mass accretion rate, above which there exists no steady solution.

2.2. Basic Equations for Perturbations

The formulation is essentially based on the spherical coordinates (r, θ, ϕ) . In order to treat a variable outer boundary position, however, we adopt a new variable x instead of r as follows,

$$x = \frac{r - r_\nu}{r_s - r_\nu}, \quad (1)$$

where r_s and r_ν denote, respectively, the radii of the shock front and of the inner boundary, which corresponds to the neutrino sphere. The time-dependent Euler equations are expressed as

$$\begin{aligned} \frac{\partial \rho}{\partial t} - \frac{x}{r_s - r_\nu} \frac{\partial r_s}{\partial t} \frac{\partial \rho}{\partial x} + \frac{\rho}{r_s - r_\nu} \frac{\partial u_r}{\partial x} + \frac{u_r}{r_s - r_\nu} \frac{\partial \rho}{\partial x} \\ + \frac{2\rho u_r}{r} + \frac{\rho}{r} \frac{\partial u_\theta}{\partial \theta} + \frac{\cot \theta \rho u_\theta}{r} + \frac{\rho}{r \sin \theta} \frac{\partial u_\phi}{\partial \phi} = 0, \end{aligned} \quad (2)$$

$$\frac{\partial u_r}{\partial t} - \frac{x}{r_s - r_\nu} \frac{\partial r_s}{\partial t} \frac{\partial u_r}{\partial x} + \frac{u_r}{r_s - r_\nu} \frac{\partial u_r}{\partial x} + \frac{1}{r_s - r_\nu} \frac{1}{\rho} \frac{\partial p}{\partial x} + \frac{GM}{r^2} = 0, \quad (3)$$

$$\frac{\partial u_\theta}{\partial t} + \frac{u_r}{r_s - r_\nu} \frac{\partial u_\theta}{\partial x} + \frac{u_r u_\theta}{r} + \frac{1}{r \rho} \frac{\partial p}{\partial \theta} - \frac{1}{r \rho} \frac{x}{r_s - r_\nu} \frac{\partial r_s}{\partial \theta} \frac{\partial p}{\partial x} = 0, \quad (4)$$

$$\frac{\partial u_\phi}{\partial t} + \frac{u_r}{r_s - r_\nu} \frac{\partial u_\phi}{\partial x} + \frac{u_r u_\phi}{r} + \frac{1}{r \rho} \frac{\partial p}{\partial \phi} - \frac{1}{r \rho} \frac{x}{r_s - r_\nu} \frac{\partial r_s}{\partial \phi} \frac{\partial p}{\partial x} = 0, \quad (5)$$

$$\frac{\partial S}{\partial t} - \frac{x}{r_s - r_\nu} \frac{\partial r_s}{\partial t} \frac{\partial S}{\partial x} + \frac{u_r}{r_s - r_\nu} \frac{\partial S}{\partial x} = \frac{\dot{q}}{\rho T}, \quad (6)$$

$$\frac{\partial Y_e}{\partial t} - \frac{x}{r_s - r_\nu} \frac{\partial r_s}{\partial t} \frac{\partial Y_e}{\partial x} + \frac{u_r}{r_s - r_\nu} \frac{\partial Y_e}{\partial x} = \frac{\lambda}{n}, \quad (7)$$

where u_r, u_θ, u_ϕ stand for the velocity components and ρ, p, S, Y_e and n represent the density, pressure, entropy per unit mass, electron fraction and baryon number density, respectively; G is the gravitational constant and \dot{M} is the mass accretion rate, which is also constant in time; M is the enclosed mass; \dot{q} and λ are the net heating and reaction rates for the absorptions and emissions of neutrinos on free nucleons. Terms result from unorthogonality of the new coordinate system is dropped here, because they are quantities of higher order of the deviation from the steady solution.

The formulation is again Newtonian and the rotation and magnetic field were neglected. Since the perturbed flows are also optically thin for neutrinos in the region of interest, the neutrino transport was ignored. In addition, we neglected the perturbations of the self-gravity of the accretion flows. This is justified from the fact that the inclusion of the self-gravity did not change much the unperturbed steady solutions except for the case with the neutrino luminosity very close to the critical value (see figure 3b in Yamasaki & Yamada (2006)). As will become clear later, the latter case is of no importance in reality.

The Rankine-Hugoniot relations at the outer boundary are expressed as

$$\rho(\mathbf{u} - \mathbf{u}_s) \cdot \mathbf{n} = \rho_u(\mathbf{u}_u - \mathbf{u}_s) \cdot \mathbf{n}, \quad (8)$$

$$(\mathbf{u} - \mathbf{u}_s) \cdot \mathbf{t}_\alpha = (\mathbf{u}_u - \mathbf{u}_s) \cdot \mathbf{t}_\alpha, \quad (9)$$

$$(\mathbf{u} - \mathbf{u}_s) \cdot \mathbf{t}_\beta = (\mathbf{u}_u - \mathbf{u}_s) \cdot \mathbf{t}_\beta, \quad (10)$$

$$\rho \left\{ (\mathbf{u} - \mathbf{u}_s) \cdot \frac{\mathbf{n}}{|\mathbf{n}|} \right\}^2 + p = \rho_u \left\{ (\mathbf{u}_u - \mathbf{u}_s) \cdot \frac{\mathbf{n}}{|\mathbf{n}|} \right\}^2 + p_u, \quad (11)$$

$$\frac{1}{2} \left\{ (\mathbf{u} - \mathbf{u}_s) \cdot \frac{\mathbf{n}}{|\mathbf{n}|} \right\}^2 + \epsilon + \frac{p}{\rho} = \frac{1}{2} \left\{ (\mathbf{u}_u - \mathbf{u}_s) \cdot \frac{\mathbf{n}}{|\mathbf{n}|} \right\}^2 + \epsilon_u + \frac{p_u}{\rho_u}, \quad (12)$$

where \mathbf{u}_s and ϵ are the shock velocity and specific internal energy, respectively; The suffix u stands for the quantities in the upstream, which was assumed to be free fall and cold; The vectors normal and tangent to the shock surface are denoted as \mathbf{n} and \mathbf{t}_α , \mathbf{t}_β , respectively, and are given as

$$\mathbf{n} = \left(1, -\frac{1}{r_s} \frac{\partial r_s}{\partial \theta}, -\frac{1}{r_s \sin \theta} \frac{\partial r_s}{\partial \phi} \right), \quad (13)$$

$$\mathbf{t}_\alpha = \left(\frac{\partial r_s}{\partial \theta}, r_s, 0 \right), \quad (14)$$

$$\mathbf{t}_\beta = \left(\frac{1}{\sin \theta} \frac{\partial r_s}{\partial \phi}, 0, r_s \right). \quad (15)$$

For the linear analysis, we employed the formulation based on the Eulerian perturbation at the fixed x -coordinate. The deviations from the unperturbed states are expanded with spherical harmonics, $Y_\ell^m(\theta, \phi)$, and are assumed to have a time dependence of $\exp(\omega t)$. Attaching the subscript 0 to the unperturbed variables and the subscript 1 to the deviations from them of the perturbed counterparts, we expressed, for example, the radial velocity as

$$u_r = u_{r0}(x) + \sum_{\ell, m} u_{r1}(x) Y_\ell^m(\theta, \phi) e^{\omega t}. \quad (16)$$

The exceptions are u_θ and u_ϕ , which were expanded with the vector spherical harmonics as

$$\begin{pmatrix} u_\theta \\ u_\phi \end{pmatrix} = \sum_{\ell,m} u_{h1}(x) \begin{pmatrix} \frac{\partial Y_\ell^m(\theta, \phi)}{\partial Y_\ell^m(\theta, \phi)} \\ \frac{\sin \theta \partial \phi}{\sin \theta \partial \phi} \end{pmatrix} e^{\omega t}. \quad (17)$$

Then the basic equations describing the perturbations to the lowest order are given for each ℓ as follows:

$$\begin{aligned} \frac{\partial(\rho_1/\rho_0)}{\partial x} + \frac{\partial(u_{r1}/u_{r0})}{\partial x} + \frac{r_{s0} - r_\nu}{u_{r0}} \omega \frac{\rho_1}{\rho_0} - \ell(\ell + 1) \frac{r_{s0} - r_\nu}{r} \frac{u_{h1}}{u_{r0}} \\ - \left[\left(\frac{\partial \ln \rho_0}{\partial x} + \frac{\partial \ln |u_{r0}|}{\partial x} \right) \frac{r_{s0}}{r_{s0} - r_\nu} + \left\{ \frac{\omega}{u_{r0}} \frac{\partial \ln \rho_0}{\partial x} + \frac{2(r_{s0} - r_\nu)}{r^2} \right\} x r_{s0} \right] \frac{r_{s1}}{r_{s0}} = 0, \end{aligned} \quad (18)$$

$$\begin{aligned} \frac{\partial(u_{r1}/u_{r0})}{\partial x} + \frac{p_0}{u_{r0}^2 \rho_0} \left(\frac{\partial \ln p}{\partial \ln \rho} \right)_0 \frac{\partial(\rho_1/\rho_0)}{\partial x} + \frac{p_0}{u_{r0}^2 \rho_0} \left(\frac{\partial \ln p}{\partial \ln S} \right)_0 \frac{\partial(S_1/S_0)}{\partial x} + \frac{p_0}{u_{r0}^2 \rho_0} \left(\frac{\partial \ln p}{\partial \ln Y_e} \right)_0 \frac{\partial(Y_{e1}/Y_{e0})}{\partial x} \\ + \left(\frac{r_{s0} - r_\nu}{u_{r0}} \omega + 2 \frac{\partial \ln |u_{r0}|}{\partial x} \right) \frac{u_{r1}}{u_{r0}} + \left\{ \frac{\partial \ln \rho_0}{\partial x} \frac{\rho_0^2}{p_0} \left(\frac{\partial^2 p}{\partial \rho^2} \right)_0 - \left(\frac{\partial \ln p}{\partial \ln S} \right)_0 \frac{\partial \ln S_0}{\partial x} \right. \\ \left. + \frac{\partial \ln S_0}{\partial x} \frac{\rho_0 S_0}{p_0} \left(\frac{\partial^2 p}{\partial \rho \partial S} \right)_0 - \left(\frac{\partial \ln p}{\partial \ln Y_e} \right)_0 \frac{\partial \ln Y_{e0}}{\partial x} + \frac{\partial \ln Y_{e0}}{\partial x} \frac{\rho_0 Y_{e0}}{p_0} \left(\frac{\partial^2 p}{\partial \rho \partial Y_e} \right)_0 \right\} \frac{p_0}{u_{r0}^2 \rho_0} \frac{\rho_1}{\rho_0} \\ + \left\{ \frac{\partial \ln \rho_0}{\partial x} \frac{\rho_0 S_0}{p_0} \left(\frac{\partial^2 p}{\partial \rho \partial S} \right)_0 + \left(\frac{\partial \ln p}{\partial \ln S} \right)_0 \frac{\partial \ln S_0}{\partial x} + \frac{\partial \ln S_0}{\partial x} \frac{S_0^2}{p_0} \left(\frac{\partial^2 p}{\partial S^2} \right)_0 \right. \\ \left. + \frac{\partial \ln Y_{e0}}{\partial x} \frac{S_0 Y_{e0}}{p_0} \left(\frac{\partial^2 p}{\partial S \partial Y_e} \right)_0 \right\} \frac{p_0}{u_{r0}^2 \rho_0} \frac{S_1}{S_0} \\ + \left\{ \frac{\partial \ln \rho_0}{\partial x} \frac{\rho_0 Y_{e0}}{p_0} \left(\frac{\partial^2 p}{\partial \rho \partial Y_e} \right)_0 + \frac{\partial \ln S_0}{\partial x} \frac{S_0 Y_{e0}}{p_0} \left(\frac{\partial^2 p}{\partial S \partial Y_e} \right)_0 + \left(\frac{\partial \ln p}{\partial \ln Y_e} \right)_0 \frac{\partial \ln Y_{e0}}{\partial x} \right. \\ \left. + \frac{\partial \ln Y_{e0}}{\partial x} \frac{Y_{e0}^2}{p_0} \left(\frac{\partial^2 p}{\partial Y_e^2} \right)_0 \right\} \frac{p_0}{u_{r0}^2 \rho_0} \frac{Y_{e1}}{Y_{e0}} \\ - \left\{ \frac{\omega}{u_{r0}} \frac{\partial \ln |u_{r0}|}{\partial x} + \frac{2(r_{s0} - r_\nu) GM}{r^3 u_{r0}^2} \right\} x r_{s0} \frac{r_{s1}}{r_{s0}} \\ - \left[\frac{\partial \ln |u_{r0}|}{\partial x} + \left\{ \left(\frac{\partial \ln p}{\partial \ln \rho} \right)_0 \frac{\partial \ln \rho_0}{\partial x} + \left(\frac{\partial \ln p}{\partial \ln S} \right)_0 \frac{\partial \ln S_0}{\partial x} + \left(\frac{\partial \ln p}{\partial \ln Y_e} \right)_0 \frac{\partial \ln Y_{e0}}{\partial x} \right\} \frac{p_0}{u_{r0}^2 \rho_0} \right] \\ \times \frac{r_{s0}}{r_{s0} - r_\nu} \frac{r_{s1}}{r_{s0}} = 0, \end{aligned} \quad (19)$$

$$\begin{aligned} \frac{\partial(u_{h1}/u_0)}{\partial x} + \left(\frac{r_{s0} - r_\nu}{u_{r0}} \omega + \frac{r_{s0} - r_\nu}{r} + \frac{\partial \ln |u_{r0}|}{\partial x} \right) \frac{u_{h1}}{u_{r0}} \\ + \frac{r_{s0} - r_\nu}{r} \frac{p_0}{u_{r0}^2 \rho_0} \left\{ \left(\frac{\partial \ln p}{\partial \ln \rho} \right)_0 \frac{\rho_1}{\rho_0} + \left(\frac{\partial \ln p}{\partial \ln S} \right)_0 \frac{S_1}{S_0} + \left(\frac{\partial \ln p}{\partial \ln Y_e} \right)_0 \frac{Y_{e1}}{Y_{e0}} \right\} \end{aligned}$$

$$-\frac{1}{r} \frac{p_0}{u_{r0}^2 \rho_0} \frac{\partial \ln p_0}{\partial x} x r_{s0} \frac{r_{s1}}{r_{s0}} = 0, \quad (20)$$

$$\begin{aligned} & \frac{\partial(S_1/S_0)}{\partial x} - \frac{r_{s0} - r_\nu}{S_0 u_{r0} \rho_0 T_0} \left\{ \rho_0 \left(\frac{\partial \dot{q}}{\partial \rho} \right)_0 - \left(\frac{\partial \ln T}{\partial \ln \rho} \right)_0 \dot{q}_0 - \dot{q}_0 \right\} \frac{\rho_1}{\rho_0} + \frac{\partial \ln S_0}{\partial x} \frac{u_{r1}}{u_{r0}} \\ & + \left[\frac{r_{s0} - r_\nu}{u_{r0}} \omega + \frac{\partial \ln S_0}{\partial x} - \frac{r_{s0} - r_\nu}{S_0 u_{r0} \rho_0 T_0} \left\{ S_0 \left(\frac{\partial \dot{q}}{\partial S} \right)_0 - \left(\frac{\partial \ln T}{\partial \ln S} \right)_0 \dot{q}_0 \right\} \right] \frac{S_1}{S_0} \\ & - \frac{r_{s0} - r_\nu}{S_0 u_{r0} \rho_0 T_0} \left\{ Y_{e0} \left(\frac{\partial \dot{q}}{\partial Y_e} \right)_0 - \left(\frac{\partial \ln T}{\partial \ln Y_e} \right)_0 \dot{q}_0 \right\} \frac{Y_{e1}}{Y_{e0}} \\ & - \left\{ \frac{\partial \ln S_0}{\partial x} \frac{r_{s0}}{r_{s0} - r_\nu} + \left(\frac{\omega}{u_{r0}} \frac{\partial \ln S_0}{\partial x} + \frac{r_{s0} - r_\nu}{S_0 u_{r0} \rho_0 T_0} \frac{\partial \dot{q}_0}{\partial r} \right) x r_{s0} \right\} \frac{r_{s1}}{r_{s0}} \\ & - \frac{r_{s0} - r_\nu}{S_0 u_{r0} \rho_0 T_0} T_{\nu0} \left(\frac{\partial \dot{q}}{\partial T_\nu} \right)_0 \frac{T_{\nu1}}{T_{\nu0}} = 0, \end{aligned} \quad (21)$$

$$\begin{aligned} & \frac{\partial(Y_{e1}/Y_{e0})}{\partial x} + \frac{\partial \ln Y_{e0}}{\partial x} \frac{u_{r1}}{u_{r0}} - \frac{r_{s0} - r_\nu}{Y_{e0} n_0 u_{r0}} \rho_0 \left(\frac{\partial \lambda}{\partial \rho} \right)_0 \frac{\rho_1}{\rho_0} - \frac{r_{s0} - r_\nu}{Y_{e0} n_0 u_{r0}} S_0 \left(\frac{\partial \lambda}{\partial S} \right)_0 \frac{S_1}{S_0} \\ & + \left\{ \frac{r_{s0} - r_\nu}{u_{r0}} \omega + \frac{\partial \ln Y_{e0}}{\partial x} - \frac{r_{s0} - r_\nu}{Y_{e0} n_0 u_{r0}} Y_{e0} \left(\frac{\partial \lambda}{\partial Y_e} \right)_0 \right\} \frac{Y_{e1}}{Y_{e0}} \\ & - \left\{ \left(\frac{\omega}{u_{r0}} \frac{\partial \ln Y_{e0}}{\partial x} + \frac{r_{s0} - r_\nu}{Y_{e0} n_0 u_{r0}} \frac{\partial \lambda_0}{\partial r} \right) x r_{s0} + \frac{\partial \ln Y_{e0}}{\partial x} \frac{r_{s0}}{r_{s0} - r_\nu} \right\} \frac{r_{s1}}{r_{s0}} \\ & - \frac{r_{s0} - r_\nu}{Y_{e0} n_0 u_{r0}} T_{\nu0} \left(\frac{\partial \lambda}{\partial T_\nu} \right)_0 \frac{T_{\nu1}}{T_{\nu0}} + \frac{r_{s0} - r_\nu}{Y_{e0} n_0 u_{r0}} \lambda_0 \frac{n_1}{n_0} = 0, \end{aligned} \quad (22)$$

where T and T_ν denote the temperatures of matter and neutrino, respectively. The eigen values are degenerate in m for the spherically symmetric background. The index ℓ explicitly appears only in Eq. (18).

The Rankine-Hugoniot relations for the perturbed quantities are written down similarly as

$$(2\rho_{f0} u_{f0} + \omega r_{s0} \rho_{f0} - \omega r_{s0} \rho_0) \frac{r_{s1}}{r_{s0}} + \rho_0 u_{r0} \left(\frac{\rho_1}{\rho_0} + \frac{u_{r1}}{u_{r0}} \right) = 0, \quad (23)$$

$$\frac{u_{h1}}{u_{r0}} - \left(\frac{u_{f0}}{u_{r0}} - 1 \right) \frac{r_{s1}}{r_{s0}} = 0, \quad (24)$$

$$\begin{aligned} & \left\{ \frac{5}{2} \rho_{f0} u_{f0}^2 + 2\omega r_{s0} \rho_{f0} u_{f0} - 2\omega r_{s0} \rho_0 u_{r0} + \frac{3}{2} \rho_{f0} \left(\frac{\partial p}{\partial \rho} \right)_{f0} \right\} \frac{r_{s1}}{r_{s0}} \\ & + 2\rho_0 u_0^2 \frac{u_{r1}}{u_{r0}} + \left\{ \rho_0 u_{r0}^2 + \rho_0 \left(\frac{\partial p}{\partial \rho} \right)_0 \right\} \frac{\rho_1}{\rho_0} + S_0 \left(\frac{\partial p}{\partial S} \right)_0 \frac{S_1}{S_0} + Y_{e0} \left(\frac{\partial p}{\partial Y_e} \right)_0 \frac{Y_{e1}}{Y_{e0}} = 0, \end{aligned} \quad (25)$$

$$\begin{aligned}
& \left\{ \frac{1}{2} u_{f0}^2 + \omega r_{s0} u_{f0} - \omega r_{s0} u_{r0} + \frac{3}{2} \rho_{f0} \left(\frac{\partial \epsilon}{\partial \rho} \right)_{f0} + \frac{3}{2} \left(\frac{\partial p}{\partial \rho} \right)_{f0} - \frac{3}{2} \frac{p_{f0}}{\rho_{f0}} \right\} \frac{r_{s1}}{r_{s0}} \\
& + u_{r0}^2 \frac{u_{r1}}{u_{r0}} + \left\{ \rho_0 \left(\frac{\partial \epsilon}{\partial \rho} \right)_0 + \left(\frac{\partial p}{\partial \rho} \right)_0 - \frac{p_0}{\rho_0} \right\} \frac{\rho_1}{\rho_0} + \left\{ S_0 \left(\frac{\partial \epsilon}{\partial S} \right)_0 + \frac{S_0}{\rho_0} \left(\frac{\partial p}{\partial S} \right)_0 \right\} \frac{S_1}{S_0} \\
& + \left\{ Y_{e0} \left(\frac{\partial \epsilon}{\partial Y_e} \right)_0 + \frac{Y_{e0}}{\rho_0} \left(\frac{\partial p}{\partial Y_e} \right)_0 \right\} \frac{Y_{e1}}{Y_{e0}} = 0. \tag{26}
\end{aligned}$$

Note that the upstream flows are unaffected by the perturbations inside the shock because they are supersonic and no fluctuations can propagate beyond the shock front. The suffix f0 stands for the upstream values at the shock front for the free fall assumed in the unperturbed background state.

In addition, we imposed

$$u_{r1} = 0, \tag{27}$$

at the inner boundary ($x = 0$), considering that the infalling matter comes to rest on the neutron star surface that is supposed to be very close to the inner boundary. The radius of the inner boundary was also fixed in the linear analysis. Since the growth of SASI is expected to be affected by the imposed inner boundary conditions, we tried some variations of these conditions, the results of which will be discussed in Section 5.

We solved Eqs. (18)-(22) as an eigen value problem for ω , imposing the boundary conditions, Eqs. (23)-(27). The procedure is as follows. We first take a trial value of ω , set r_{s1}/r_{s0} to be unity and solve the Rankine-Hugoniot relations, Eqs. (23)-(26), and integrate Eqs. (18)-(22) from the outer boundary down to the inner boundary. The solution obtained this way does not, in general, meet the inner boundary condition, Eq. (27). Then we improve the value of ω and repeat the procedure until Eq. (27) is satisfied at the inner boundary by the solution.

3. Eigen Frequencies of Various Modes

In this section, we summarily present various modes that we found in this paper. The detailed analysis of each mode will be given in the following sections. We show only the results for $\dot{M} = 1.0 M_{\odot}/\text{s}$, since their quantitative nature is weakly dependent on the value of mass accretion rate. Unlike the previous paper (Yamasaki & Yamada 2005), in this and next sections, the neutrino temperature is assumed to be unperturbed, that is, $T_{\nu 1} = 0$. This is also equivalent to the negligence of the perturbation of neutrino luminosity. The underlying idea is that the neutrino luminosity is dominated by the contribution from the proto neutron star rather than from the accreted matter. The influence of the perturbation

of neutrino luminosity will be considered separately in section 5. We explored all the modes of relevance below the critical neutrino luminosity, which is 124.801×10^{51} ergs/s for the mass accretion rate given above.

First, we consider the radial modes with $\ell = 0$. It is noted that the stability of spherical accretion flows against radial modes were investigated by several authors (Nakayama 1992, 1993, 1994; Houck & Chevalier 1992; Foglizzo & Tagger 2000; Foglizzo 2001, 2002; Yamasaki & Yamada 2005) in different contexts. Nakayama (1992, 1993, 1994), for example, showed that the isothermal or adiabatic transonic accretion flows around black hole are unstable when the postshock flow is accelerated. The effect of cooling was investigated by Houck & Chevalier (1992) for the accretion flows to neutron stars or white dwarfs with a use of a simple analytic form of cooling. Yamasaki & Yamada (2005) analyzed the linear stability of spherically symmetric subsonic accretion flows from a standing shock down to a proto neutron star, using an analytic form of heating and cooling by neutrinos taken into account. This paper is an extention of Yamasaki & Yamada (2005) to the models with more realistic neutrino heating/cooling and equation of state that are appropriate for the post-bounce phase of core-collapse supernovae (see also Yamasaki & Yamada (2006)).

The results are shown in Fig. 1, where the real and imaginary parts of ω (see Eq. (16)) are displayed for representative radial modes. It is found from the right panel that there are both oscillatory ($\text{Im}(\omega) \neq 0$) and non-oscillatory ($\text{Im}(\omega) = 0$) modes. The mode shown with a long-dashed line is non-oscillatory and stable ($\text{Re}(\omega) < 0$) for all the luminosities with no radial node. We distinguish the eigen modes with similar features by the number of radial nodes. We refer to the eigen mode with the smallest number of radial nodes, normally none or one, as a fundamental mode of the family. The modes with the second and third smallest number of radial nodes are called the first and second overtones, respectively. In this notation, the above mentioned mode is a fundamental mode. This mode is of thermal nature in the sense that it disappears if the perturbations of the heating rates are neglected, and has no non-radial counterpart. More importantly, this corresponds to the mode that was discussed in Yamasaki & Yamada (2005) and made the outer solutions unstable and, as a result, rendered the critical solution marginally unstable. It is interesting to point out that the mode is not unstable even marginally at the critical luminosity. This is simply because the neutrino-luminosity perturbations are ignored. This issue will be discussed further in detail in section 5.

It is apparent from Fig. 1 that the radial stability is much more complicated in the present models than in those considered in Yamasaki & Yamada (2005). In fact, besides the thermal modes just discussed, we found oscillatory modes shown with solid and dashed lines in the figure. These are the fundamental and first overtone modes. This complexity

is originated from the non-monotonic background flows obtained for the realistic neutrino heating rates and equation of state. We refer readers to Yamasaki & Yamada (2006) for more details on the unperturbed states. While the first overtone (the dotted line) is stable and oscillatory for all the luminosities up to the critical value, the fundamental mode becomes unstable when the luminosity is larger than $\sim 7 \times 10^{52}$ ergs/s. For the luminosities greater than $\sim 9 \times 10^{52}$ ergs/s, the mode bifurcates into two branches and become non-oscillatory. Although both the non-oscillatory modes are unstable, one of them is almost neutral for most of the luminosities. The overstablizing radial mode that exists for the luminosities $\lesssim 9 \times 10^{52}$ ergs/s was not found in Yamasaki & Yamada (2005) but observed in the numerical simulations by Ohnishi et al. (2006) and the reason was not clear in the latter paper.

We can now ascribe the apparent discrepancy to the difference of the implemented microphysics. In fact, we re-examined the models with the simplified neutrino-heating rates and equation of state employed in Yamasaki & Yamada (2005) and found that the same mode exists in this case also indeed, but it is stable up to the critical luminosity. In Yamasaki & Yamada (2005), the critical luminosity was reached before the present mode becomes unstable. In other words, which mode becomes unstable for smaller neutrino luminosities, the present mode or the thermal mode, is dependent on the background model, which is in turn determined by the adopted microphysics. The oscillatory instability seems to be driven by the advection-acoustic cycles (Foglizzo & Tagger 2000; Foglizzo 2001). As shown in Fig. 4 together with other non-radial modes that will be discussed later, the oscillation frequency agrees with the period of the advection-acoustic cycle rather well. As will be described shortly, the non-radial modes become unstable for smaller neutrino luminosities than these radial unstable modes. Hence the latter modes will be of little practical importance. Other than the modes mentioned above, we did not find any unstable radial modes.

Next we pay attention to the stability of accretion flows against non-radial perturbations. Foglizzo & Tagger (2000); Foglizzo (2001, 2002) conducted global linear analyses on the stability of black hole accretions, using a polytropic equation of state. They claimed that the origin of the instability is a repeated coupling of inward-advection vortices and entropy perturbations with outward-propagating acoustic waves. It should be noted that the results cannot be directly applied to the post-bounce flows in the supernova core of our current interest. While in the the black hole accretion the flow is transonic and the inner boundary is the event horizon, in the latter case the flow is subsonic and there is a surface of proto neutron star at the inner boundary. Galletti & Foglizzo (2005) attempted a linear analysis more appropriate for the supernova core but with a polytopic equation of state and a simple analytic cooling term. Several numerical studies were also performed (Blondin et al. 2003; Scheck et al. 2004; Blondin & Mezzacappa 2006; Ohnishi et al. 2006), and they all found the growths of unstable modes with $\ell = 1$ and 2.

The results of our calculations are shown in Figs. 2 and 3, where the growth rates and oscillation frequencies of the fundamental and first three overtone modes are given for $\ell=1-4$. All the modes are oscillatory ($\text{Im}(\omega) \neq 0$) for small neutrino luminosities $\lesssim 7 \times 10^{52}$ ergs/s. The accretion flows are stable against all the non-radial modes if the neutrino luminosity is $\lesssim 1 \times 10^{52}$ ergs/s for the present model with $\dot{M} = 1.0 M_{\odot}/\text{s}$. For larger luminosities, the first overtones of $\ell = 2$ and 3 modes become unstable at first for relatively low neutrino luminosities, $2 \sim 3 \times 10^{52}$ ergs/s, whereas the fundamental modes with $\ell = 1$ and 2 become unstable for a bit higher luminosities, $3 \sim 7 \times 10^{52}$ ergs/s, with the former more unstable. For $\ell > 3$, there is no unstable oscillatory mode. For still larger luminosities, $\gtrsim 7 \times 10^{52}$ ergs/s, the fundamental modes of all ℓ 's become non-oscillatory ($\text{Im}(\omega) = 0$) and unstable. It is interesting that they split into two different modes at the same neutrino luminosity. These features are quite similar to the radial fundamental modes, but are sensitive to the treatment of neutrino-luminosity perturbations, which will be discussed in section 5.

4. Mechanisms of Instabilities

We now discuss the nature of each mode more in detail. In the previous section, we found both oscillatory and non-oscillatory modes. In the following, we treat them separately.

4.1. Oscillatory Modes — Advection-Acoustic Cycle or Purely Acoustic Cycle?

As shown in the previous section, all the modes except for the radial fundamental thermal mode are oscillatory for low neutrino luminosities. Although most of them are decaying oscillators, some of them, e.g. the fundamental modes of $\ell = 0, 1$ and the first overtones of $\ell = 2, 3$ modes, become growing oscillators at a certain neutrino luminosity that is specific to each mode. Recently, Blondin & Mezzacappa (2006) and Ohnishi et al. (2006) did 2D numerical experiments on the instability of the accretion flows onto a proto neutron star and observed the non-radial oscillatory instabilities. Moreover, Ohnishi et al. (2006) found the oscillating radial mode that had not been expected in the paper by Yamasaki & Yamada (2005) as mentioned in section 3. Although the oscillation frequencies were consistent with each other, these authors preferred a different interpretation on the mechanism of the instabilities. While Ohnishi et al. (2006) supported the advection-acoustic-cycle mechanism proposed by Foglizzo & Tagger (2000); Foglizzo (2001), Blondin & Mezzacappa (2006) claimed that the purely acoustic cycles were responsible for the instabilities. In order to shed light on this issue, we pay attention in this section to the possible origin of the oscillations.

We first compare a couple of frequencies of relevance. We define the time scales of the advection-acoustic cycle, τ_{aa} , and purely acoustic cycle, τ_{pa} , along the radial path as follows,

$$\tau_{\text{aa}} \equiv \int_{r_\nu}^{r_s} \left(\frac{1}{c_s + u_r} - \frac{1}{u_r} \right) dr, \quad (28)$$

$$\tau_{\text{pa}} \equiv \int_{r_\nu}^{r_s} \left(\frac{1}{c_s + u_r} + \frac{1}{c_s - u_r} \right) dr, \quad (29)$$

where c_s is the sound speed. These frequencies are displayed together with the oscillation frequencies obtained for various modes in Fig. 4. We can see that $2\pi/\tau_{\text{aa}}$, the characteristic frequency of the advection-acoustic cycle, agrees rather well with the oscillation frequencies of the radial and non-radial modes whereas the characteristic frequency for the acoustic cycle along the radial path, $2\pi/\tau_{\text{pa}}$, is much larger. In fact, τ_{aa} is almost coincident with the oscillation frequency of the radial oscillatory mode. Blondin & Mezzacappa (2006) insisted that the sound propagation is not radial for $\ell \neq 0$ modes. For comparison, we also calculated the characteristic frequency for the sound wave to travel around along the shock front although such a propagation of sound wave is highly unlikely, since the radial gradient of the sound velocity is negative and the sound wave will be deflected outwards like seismic waves. This frequency is in better agreement with the oscillation frequencies than τ_{pa} , but appears to be too small compared with the oscillation frequencies for low neutrino luminosities, particularly when the modes are unstable. For these low luminosities, the shock front is close to the inner boundary and the radial path is much shorter than the circular path, and, as a result, the difference of the interpretations is expected to be most remarkable. Note that the round-trip frequency becomes closer to the oscillation frequencies at the lowest luminosities. This is due to the non-monotonic radial dependence of sound velocity at these luminosities, where the vicinity of the shock front has the largest sound speed. These results, although not conclusive, seem to support the advection-acoustic-cycle origin of the oscillation frequencies

Next, we discuss whether the advection of entropy- and velocity perturbations and the propagation of pressure fluctuations actually occur in our models. In Figs. 5 and 6 shown are the eigen functions of the oscillatory modes of $\ell = 1, 2$. In drawing these figures, we changed the radial coordinate from x to r so that the Eulerian perturbations of variables for fixed r could be obtained. For example, this Eulerian perturbation of u_r denoted by the prime is related with another Eulerian perturbation for fixed x by the following relation.

$$u'_r \equiv u_{r1} - x r_{s1} \frac{du_{r0}}{dr}. \quad (30)$$

Note that the luminosities are chosen so that the displayed modes are unstable, $\text{Re}(\omega) > 0$. The eigen functions are complex quantities in general and both the real and imaginary part are presented in the figures.

In order to see if a particular fluctuation is propagated inward or outward, we calculated the "phase" of the perturbed quantity defined, for example, for the horizontal velocity as follows:

$$\phi \equiv \arccos \left(\frac{\text{Re}(u_{h1})}{|u_{h1}|} \right). \quad (31)$$

The values within $[0, 2\pi]$ are chosen at the shock front and extended continuously inwards.

In Fig. 7 given are the phases of the perturbations of pressure, horizontal velocity and entropy. We also present the corresponding amplitudes in Fig. 8. It is clear from Fig. 7 that the phases of the perturbations of the horizontal velocity and entropy increase with radius, which implies that they are propagating inward. (Note that the time-dependence of perturbation is $\exp(i\text{Im}(\omega)t)$). On the other hand, the phase of the pressure perturbation is almost constant with radius. There is a slight positive gradient in the inner region, indicating the inward propagation there, and a negative gradient in the outer region, implying the outward propagation. This observation suggests that the pressure perturbation is not only propagating outward but also inward with almost the same amplitude. It should be also mentioned that the wave length of the pressure perturbations, that is the sound velocity times the oscillation frequency, is longer than the distance between the shock wave and the inner boundary. This is also reflected in the lack of short-wave-length modulations of the amplitude for the pressure perturbation shown in Fig. 8. In such a situation, it may not be meaningful to define a propagation path of the pressure perturbation and this might be the source of difficulty in interpreting the mechanism of the instability.

From Fig. 8, we can see which inward-adverted quantity, the perturbation of entropy or horizontal velocity, could give a larger contribution to the excitation of pressure perturbations. Note that the amplitudes are normalized at the shock front. As is clear, the entropy perturbation is significantly damped from the initial value by the time it reaches the inner boundary. This is particularly the case for the fundamental mode of $\ell = 1$ at $L_{\nu_e} = 6 \cdot 10^{52}$ ergs/s. The evolution of the entropy perturbation is determined by the non-adiabatic processes, that is the heating and cooling by neutrinos. A similar damping of the entropy perturbation is also seen for the first overtone of $\ell = 2$ mode at $L_{\nu_e} = 3 \cdot 10^{52}$ ergs/s although the damping region is rather confined to the vicinity of the inner boundary. The perturbation of the horizontal velocity, on the other hand, is not reduced significantly as it is advected inward regardless of the unstable modes. Hence, if it is the advection-acoustic cycle that drives the instability, the vortices rather than the entropy fluctuations will be the dominant source of the excitation of pressure perturbations. It is incidentally mentioned that the pressure perturbation is also damped rather rapidly as it propagates outward as shown in Fig. 8.

In our models meant for the core-collapse supernovae, the unstable modes induced

supposedly by the vortex-acoustic cycle have lower oscillation frequencies compared with the models meant for the black hole accretion by Foglizzo (2001, 2002). This difference comes from the condition satisfied at the inner boundary, around which the excitation of acoustic waves takes place most efficiently. (See Foglizzo & Galletti (2004) for the physical interpretation.) Whereas the inflow velocity approaches the sound velocity at the inner boundary in the case of the black hole accretion, the flow is highly subsonic near the inner boundary in the present case, which lead to the observed lower frequencies of the unstable oscillations induced by advected vortices in our models.

4.2. Non-Oscillatory Modes — Convective Instability

As shown in the previous section, when the luminosity is larger than about 7×10^{52} ergs/s, there exist non-oscillatory unstable modes for all ℓ 's including $\ell = 0$. (see Figs. 1 and 2.) Although the dependence of the growth rate on the neutrino luminosity looks similar for these unstable modes, the eigen functions of the non-radial modes ($\ell \neq 0$) are qualitatively different from that of the radial mode ($\ell = 0$). This can be seen in Fig. 9, where the eigen functions of the modes with $\ell=0-4$ are displayed and the gain radius is marked by the thin dotted lines. While the eigen function of the entropy perturbation for the radial mode has no node, those for the non-radial modes have a node near the gain radius. The eigen functions of the radial-velocity perturbation also show a difference between them; they take the maximum absolute value near the gain radius for the non-radial modes, whereas a rather monotonic decay is seen for the radial mode as the radius decreases. The fact that the heating region between the shock and the gain radius has a negative entropy gradient and that these unstable non-radial modes appear to be excited in this region suggests that they are convective modes. (The radial mode cannot be the convective mode in nature).

The growth rates of the convective modes together with the radial mode are demonstrated in Fig. 10. When the luminosity becomes greater than $\sim 7 \times 10^{52}$ ergs/s, all the modes are bifurcated into two branches. Although this behavior is common to the radial mode, it is apparent from the left panel of this figure that the radial mode does not belong to the same family. In the right panels, the ℓ -dependences of the growth rate (upper panel) and the luminosity (lower panel), at which the mode with a given ℓ becomes unstable for the first time, are shown. The growth rate increases at first and then decreases as ℓ becomes larger. The peak occurs at $\ell = 5 - 11$, depending on the neutrino luminosity. On the other hand, the luminosity, at which the convective instability appears, decreases with ℓ at first until $\ell = 6$ and then it increases. These peaks are rather broad, and a couple of modes become unstable almost at the same luminosity with similar growth rates.

As shown in the previous paper (Yamasaki & Yamada 2005, 2006), there appears a heating region in the accretion flow for the luminosity larger than a certain value. It is easy to see that the heating region, if exists, has a negative entropy gradient. In such a region, the conventional criterion predicts an existence of convection. In our models with the mass accretion rate of $\dot{M} = 1.0M_{\odot}/\text{s}$, the critical luminosity for the existence of the heating region is $3.7 \times 10^{52}\text{ergs/s}$. It should be emphasized here that the actual convective instability occurred at larger neutrino luminosity, $\sim 7 \times 10^{52}\text{ergs/s}$. This confirms the recent findings by Foglizzo et al. (2005) that the advection stabilizes the convective modes.

Introducing the parameter χ , which is roughly the ratio of the advection time scale and the growth time scale of convective instability, Foglizzo et al. (2005) gave the additional criterion, $\chi > 3$, for the convective instability in the advecting matter. In our previous paper (Yamasaki & Yamada 2006), we calculated the value of χ for the steady solution that is employed in the present paper, and found that the value of χ is always less than 3. If the criterion by Foglizzo et al. (2005) is applicable to our models, we should have found no unstable convective mode. The apparent discrepancy is traced back to the difference of the unperturbed models adopted for linear analysis. Foglizzo et al. (2005) assumed simplified formulae for the neutrino heating and equation of state while we employed more realistic ones and, as a result, the post-shock flows are much complicated (see Fig. 2 of Yamasaki & Yamada (2006)). Another important difference is that we considered the whole region between the standing shock and the neutrino sphere, whereas Foglizzo et al. (2005) treated only the heating region, imposing a boundary condition at the gain radius. Our models suggest that the critical value of χ for the convective instability may be as small as 0.356. Incidentally, Foglizzo et al. (2005) estimated that the growth rate is largest at $\ell = 6$, which is in rough agreement with our results although our calculations showed that the value of ℓ depends on the neutrino luminosity.

5. Dependence on the Assumptions

In this section we discuss possible changes of the results obtained so far when different perturbations of neutrino luminosity and inner boundary conditions are employed.

In the previous sections, we assumed that the neutrino temperature (and luminosity, as a result) was not affected by the perturbations. This is based on the idea that neutrino luminosity is dominated by the contribution from the proto neutron star, which is little affected by the fluctuations of accretion flows. It is noted that the neutrino temperature characterizing its spectrum does not coincide in general with the matter temperature at the neutrino sphere. It is possible, however, that the neutrino emission from the accreted matter

is more important and the fluctuation of the neutrino luminosity is correlated with the perturbation of matter temperature. Here we consider this case by imposing the condition that the variation of the neutrino temperature is proportional to that of the matter temperature, that is,

$$\frac{T_{\nu 1}}{T_{\nu 0}} = \frac{T_1}{T_0} \Big|_{r=r_\nu} . \quad (32)$$

We assumed that the temperature fluctuations given by Eq. (32) affect only the heating of the matter with the same polar and azimuthal angle (θ, ϕ) .

The results are shown in Figs. 11 and 12. We show the growth rates and oscillation frequencies for the modes with $\ell = 0-3$. Compared with the corresponding results shown in Figs. 2 and 3, the qualitative feature is unchanged. The thermal mode exists among the radial modes and is stable for all the neutrino luminosities as in the previous case. The first overtones of $\ell = 2, 3$ modes become unstable for relatively small luminosities. Then the fundamental $\ell = 1$ mode takes over. They are all oscillatory. Again above $L_{\nu e} \sim 7 \times 10^{52}$ ergs/s the fundamental modes are bifurcated into two branches and become non-oscillatory. Quantitatively, the growth rate is slightly modified with no clear tendency. The temporal variation of neutrino temperature sometimes helps the growth of the perturbations but other times not. It is determined by the integral of the fluctuations of heating over the entire cycle of the oscillation of the neutrino temperature. If the fluctuation of neutrino temperature and those of other quantities are synchronized, the perturbation is enhanced and vice versa. It should be also noted that the variation of the neutrino temperature is not necessarily synchronized with the temperature of the accreting matter at the neutrino sphere in reality.

We tried yet another case concerning the perturbation of neutrino emissions. For both cases considered thus far, the thermal mode was stable even at the critical luminosity (see the long dashed lines for the $\ell = 0$ modes in Figs. 1 and 11). As mentioned earlier, this is strange at first glance. Naively speaking, the thermal mode is expected to become neutral at the critical luminosity, where the inner solution and the outer solution coincide with each other. The reason for this is traced back to the condition that the radius of the inner boundary be unaffected by the perturbation. This excludes the mode that corresponds to the infinitesimal transformation of the outer solution to the inner solution in the close vicinity of the critical neutrino luminosity. We thus considered the variation of the inner boundary in such a way that the Lagrangian density-perturbation be zero at the inner boundary for the perturbed flows. This is exactly the same treatment we adopted in the previous paper (Yamasaki & Yamada 2005). Note that this condition is difficult to impose for non-radial modes, and we consider only the radial modes here.

The results are shown in Fig. 13. As expected, the thermal mode denoted by the long dashed curve is stable below the critical luminosity and becomes neutral at the critical point. Figure 14 is a zoom in to the critical point, and not only the inner solution but also the outer solution is displayed. Again as expected, they coincide with each other as a neutral mode at the critical luminosity. An interesting thing is that the outer solutions are also stable below the critical luminosity, contrary to the previous results by Yamasaki & Yamada (2005). This is due to the difference of the background flows. The flow just behind the shock is strongly decelerated in the present model, whereas it is slightly accelerated in the previous model. This is mainly due to the self gravity that was ignored in the previous calculations. Such a deceleration tends to stabilize the perturbations (Nakayama 1992, 1993, 1994). It is noted that the spherical accretion flows become unstable against the non-radial perturbations anyway. Another new feature is that the oscillatory radial fundamental mode (the solid curve in Fig. 13) is not bifurcated up to the critical luminosity. The temporal variations of the neutrino sphere somehow delayed the occurrence of the bifurcation. For the moment, we do not have a good explanation for this phenomenon. We do not know either whether other non-radial fundamental modes are also affected or not.

Next we consider the variation of the inner boundary condition for the radial velocity. If the repeated propagations and mutual excitations of the acoustic waves and the velocity and entropy fluctuations are responsible for the instability of accretion flows, the inner boundary condition is one of the key ingredients that may change the result qualitatively. So far we adopted the "solid" boundary condition, that is, $u_{r1} = 0$ at the inner boundary. By constraining the velocity perturbation this way, we may have enhanced the reflections of perturbations. In order to see this effect, here we adopt the "free" boundary condition that is given by

$$\frac{du_{r1}}{dr} = 0 \quad (33)$$

at the inner boundary. This made the calculation of the linear perturbations much more difficult, however. In fact, we often came across the difficulty in obtaining a sufficient convergence of iterative calculations. As a result, the eigen values that we present below have much larger numerical errors systematically, which will be inferred from the artificial fluctuations in Fig. 15. In spite of the problem, we still think that we can obtain a result that is qualitatively correct and will be helpful for the society.

In Fig. 15, we plotted the growth rates, $\text{Re}(\omega)$, for the $\ell = 1$ modes as a function of the neutrino luminosity. This should be compared with the upper left panel of Fig. 2. The qualitative behavior of the fundamental mode is similar. However, the growth rate of unstable oscillation is a bit larger and the neutrino luminosity, at which the mode becomes unstable, is a little lower than in the model with the "solid" boundary condition. This seems

to imply that the "free" inner boundary condition tends to enhance the instability, contrary to the naive expectation. This is also reflected in the behaviors of the overtones. In fact, while in the "solid" boundary case the overtone modes are almost stable up to the critical luminosity, in the "free" boundary case they are as unstable as the fundamental modes for relatively small luminosities. From these results, we can claim at least that the instability we have discussed is not an artifact of the boundary condition we imposed. It is also suggested that the excitations of acoustic waves occur not only at the inner boundary but over a wider region.

6. Summary and Discussions

In this paper, we investigated the stability of the spherically symmetric accretion flow through the standing shock wave onto the proto neutron star, which is supposed to approximate the post-bounce situation in the core-collapse supernova. We performed systematically the global linear-stability analyses for both radial and non-radial perturbations. We found that the flow is stable for all modes if the neutrino luminosity is lower than $\sim 1 \times 10^{52}$ ergs/s in our models with $\dot{M} = 1.0M_{\odot}/\text{s}$. For larger luminosities, the non-radial instabilities are induced, probably via the advection-acoustic cycles. The modes with $\ell = 2$ and 3 become unstable at first for relatively low neutrino luminosities, e.g. $\gtrsim 2 - 3 \times 10^{52}$ ergs/s for the same accretion rate, whereas the $\ell = 1$ mode is the most unstable for higher luminosities, $\sim 3 - 7 \times 10^{52}$ ergs/s. These are all oscillatory modes. For still higher luminosities, $\sim 7 \times 10^{52}$ ergs/s, the non-oscillatory modes become unstable, the non-radial ones among which we identified as convection. In this way, we discussed the convective instability in the presence of advection on the same basis. We found that the growth rates of the convective modes change gradually with ℓ and have a peak at $\ell = 5 - 11$, depending on the luminosity. The luminosity, at which each convective mode becomes unstable, decreases with ℓ up to $\ell = 6$ and then increases for the same accretion rate. We confirmed the results obtained by numerical simulations that the instabilities induced by the advection-acoustic cycles become more important than convections for lower neutrino luminosities. We modified the criterion for the convection in the presence of advection previously discussed by Foglizzo et al. (2005). Furthermore, we investigated the sensitivity of the results to the inner boundary conditions and found that the nature of the instabilities is not changed qualitatively.

In most of realistic simulations, the neutrino luminosity seems to be much smaller than the critical value (see e.g. (Janka et al. 2005; Sumiyoshi et al. 2005)). Hence, from the results of this paper, the over-stabilizing modes induced probably by the advection-acoustic cycles are more important than convections in causing the global anisotropy as observed

in the ejecta of core-collapse supernovae (Leonard et al. 2000; Wang et al. 2002). The instability is normally saturated at some amplitudes owing to the non-linear coupling of various modes (Ohnishi et al. 2006). Although the instability of the standing shock wave, whatever the cause, is helpful for the shock revival, recent multi-dimensional numerical simulations (Janka et al. 2005) demonstrated that these instabilities alone could not induce an explosion. Then there must be some other agents to further boost the shock revival. Very recently Burrows et al. (2006) proposed a new mechanism, in which the dissipation of out-going acoustic waves that are excited by g-mode oscillations in the proto neutron star is the agent of the shock revival. In this context, the possible coupling between the instabilities of the accretion flows and the oscillations of the proto neutron star are interesting (Yoshida et al. 2006; Ohnishi et al. 2006b).

In this paper, we considered only the spherically symmetric background flows. Considering the fact that massive stars are rotating in general, we are naturally concerned with the stability of rotational accretion flows. In the previous paper (Yamasaki & Yamada 2005), we showed that the rapid rotation changes steady accretion flows in such a way that the critical luminosity is decreased and, as a result, the shock revival is facilitated. In so doing, we found that some of the models have a negative entropy gradient and can be convectively unstable. From the results of this paper, we also expect some oscillatory modes will become unstable and will be more important than convection for low neutrino luminosities. Magnetic fields may also play an important role for the stability of accretion flows. Then, the so-called magneto-rotational instability (MRI) should be discussed in the same framework. In the case of the spherically symmetric background considered in this paper, each eigen value is degenerate with respect to the index, m . In the presence of rotation and/or magnetic field, the degeneracy will be removed at least partially. Furthermore, how the growth rates themselves are modified by these effects is an interesting issue. We are currently undertaking the task (Yamasaki & Yamada 2006b) and the results will be published elsewhere.

This work is partially supported by the Grant-in-Aid for the 21st century COE program "Holistic Research and Education Center for Physics of Self-organizing Systems" of Waseda University and for Scientific Research (14740166, 14079202) of the Ministry of Education, Science, Sports and Culture of Japan.

REFERENCES

Blondin, J. M., Mezzacappa, A., & DeMarino, C. 2003, ApJ, 584, 971
Blondin, J. M., & Mezzacappa, A. 2006, ApJ, 642, 401

Bruenn, A. 1988, ApJS, 58, 771

Burrows, A., & Goshy, J. 1993, ApJ, 416, L75

Burrows, A., Livne, E., Dessart, L., Ott, C.D., & Murphy, J. 2006, ApJ, 640, 878

Foglizzo, T., & Tagger, M. 2000, A&A, 363, 174

Foglizzo, T. 2001, A&A, 368, 311

Foglizzo, T. 2002, A&A, 392, 353

Foglizzo, T., & Galletti, P. 2004, *Cosmic explosions in three dimensions : asymmetries in supernovae and gamma-ray bursts. Cambridge contemporary astrophysics series.* Cambridge University Press, 2004, p.238

Foglizzo, T., Scheck, L., & Janka, H.-Th. 2005, *EdP-Sciences, Conference Series*, 2005, p. 483, (astro-ph/0507636)

Galletti, P., & Foglizzo, T. 2005, *EdP-Sciences, Conference Series*, 2005, p. 487

Heger, A., Langer, N., & Woosley, S. E. 2000, ApJ, 528, 368

Heger A, Woosley S. E., Langer N., & Spruit H. C. 2004 *Proc. IAU 215 Stellar Rotation*, p. 591

Houck, J. C., & Chevalier, R. A. 1992, ApJ, 395, 592

Howe, M. S. 1975, J. Fluid Mech., 71, 625

Janka, H. -Th., Buras, R., Kitaura Joyanes, F. S., Marek, A., Rampp, M. & Scheck, L. 2005, NPA, 758, 19

Kotake, K., Sato, K., & Takahashi, K. 2006, Rept.Prog.Phys. 69, 971-1144

Leonard, D. C., Filippenko, A. V., Barth, A. J., & Matheson, T. 2000, ApJ, 536, 239

Lyne, A. G., & Lorimer, D. R., 1994, Nature, 369, 127

Nakayama, K. 1992, MNRAS, 259, 259

Nakayama, K. 1993, PASJ, 45, 167

Nakayama, K. 1994, MNRAS, 270, 871

Ohnishi, N., Kotake K., & Yamada, S. 2006, ApJ, 641, 1018

Ohnishi, N., Kotake K., & Yamada, S. 2006b, in preparation

Scheck, L., Plewa, T., Janka, H.-Th., Kifonides, K., & Müller, E. 2004, Phys. Rev. Lett., 92, 011103

Shen, H., Toki, H., Oyamatsu, K., & Sumiyoshi, K. 1998, Nucl. Phys. A, 637, 435

Sumiyoshi, K., Yamada, S., Suzuki, S., Shen, H., Chiba, S., & Toki, H. 2005, ApJ, 629, 922

Wang, L., Wheeler, J. C., Höflich, P., Khokhlov, A., Baade, D., Branch, D., Challis, P., Filippenko, A. V., Fransson, C., Garnavich, P., Kirshner, R. P., Lundqvist, P., McRay, R., Panagia, N., Pun, C. S. J., Phillips, M. M., Sonneborn, G., & Suntzeff, N. B. 2002, ApJ, 579, 671

Yamasaki, T., & Yamada, S. 2005, ApJ, 623, 1000

Yamasaki, T., & Yamada, S. 2006, ApJ, accepted, (astro-ph/0606504)

Yamasaki, T., & Yamada, S. 2006, in preparation

Yoshida, S., Ohnishi, N., & Yamada, S. 2006b, in preparation

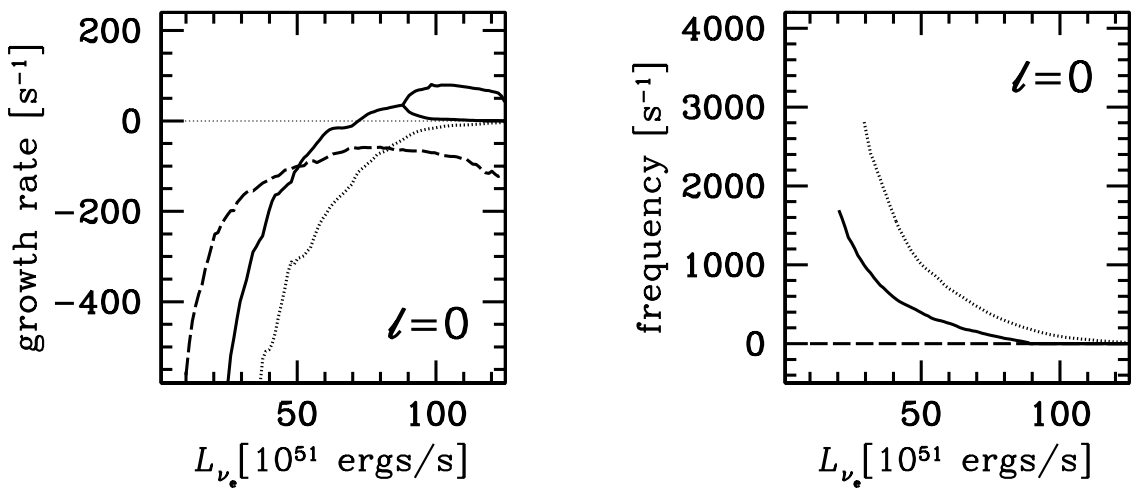


Fig. 1.— (a) The growth rates, $\text{Re}(\omega)$, and (b) oscillation frequencies, $\text{Im}(\omega)$, for representative radial ($\ell = 0$) modes as a function of neutrino luminosity. The long dashed curve denotes the fundamental thermal mode. The solid and dotted curves correspond to the fundamental and first overtone oscillatory modes, respectively.

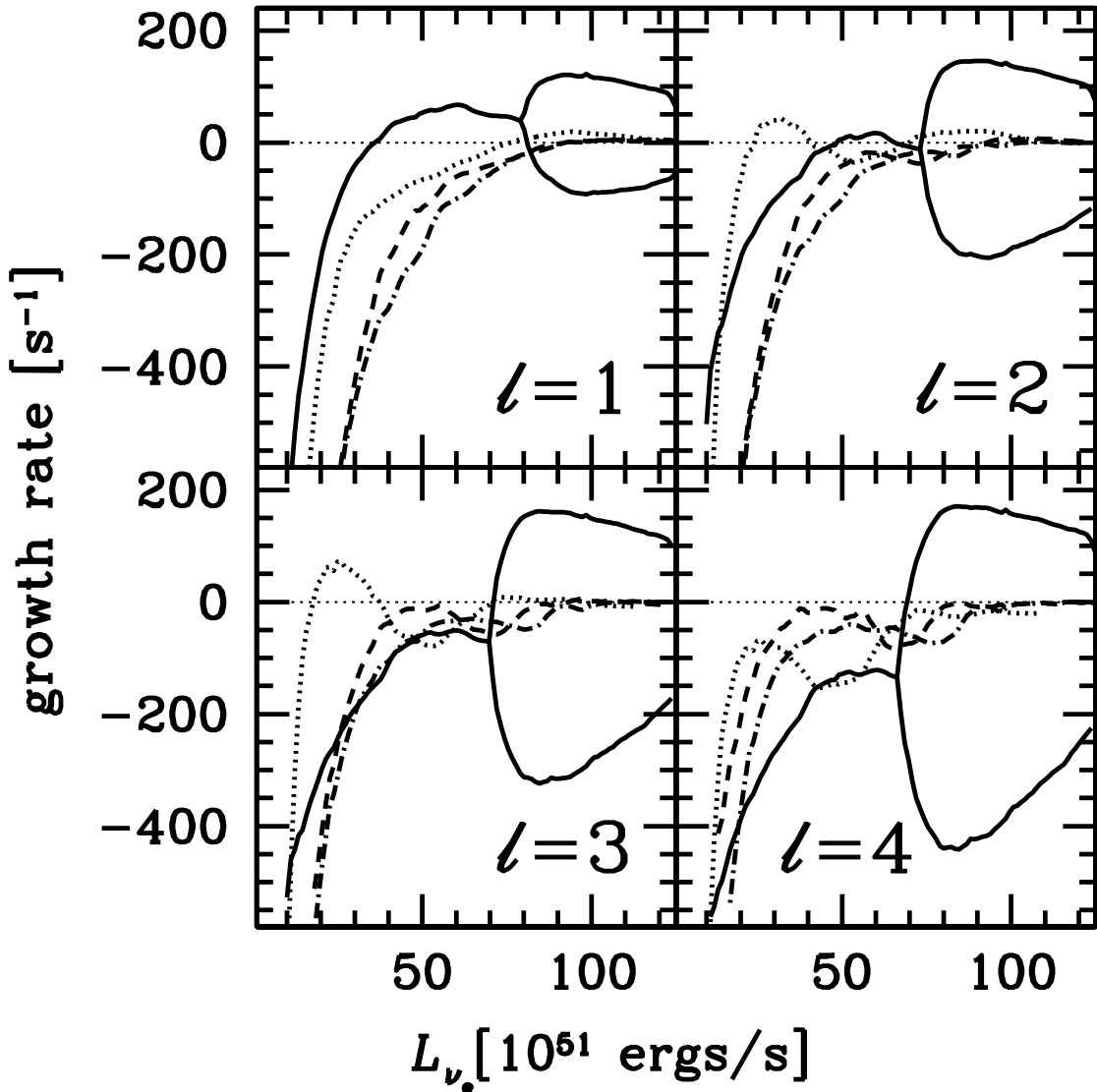


Fig. 2.— The growth rates, $\text{Re}(\omega)$, for the non-radial modes of $l = 1, 2, 3, 4$ as a function of neutrino luminosity. The solid curves represent the fundamental modes while the dotted, dashed and dash-dotted curves correspond to the first, second and third overtones, respectively.

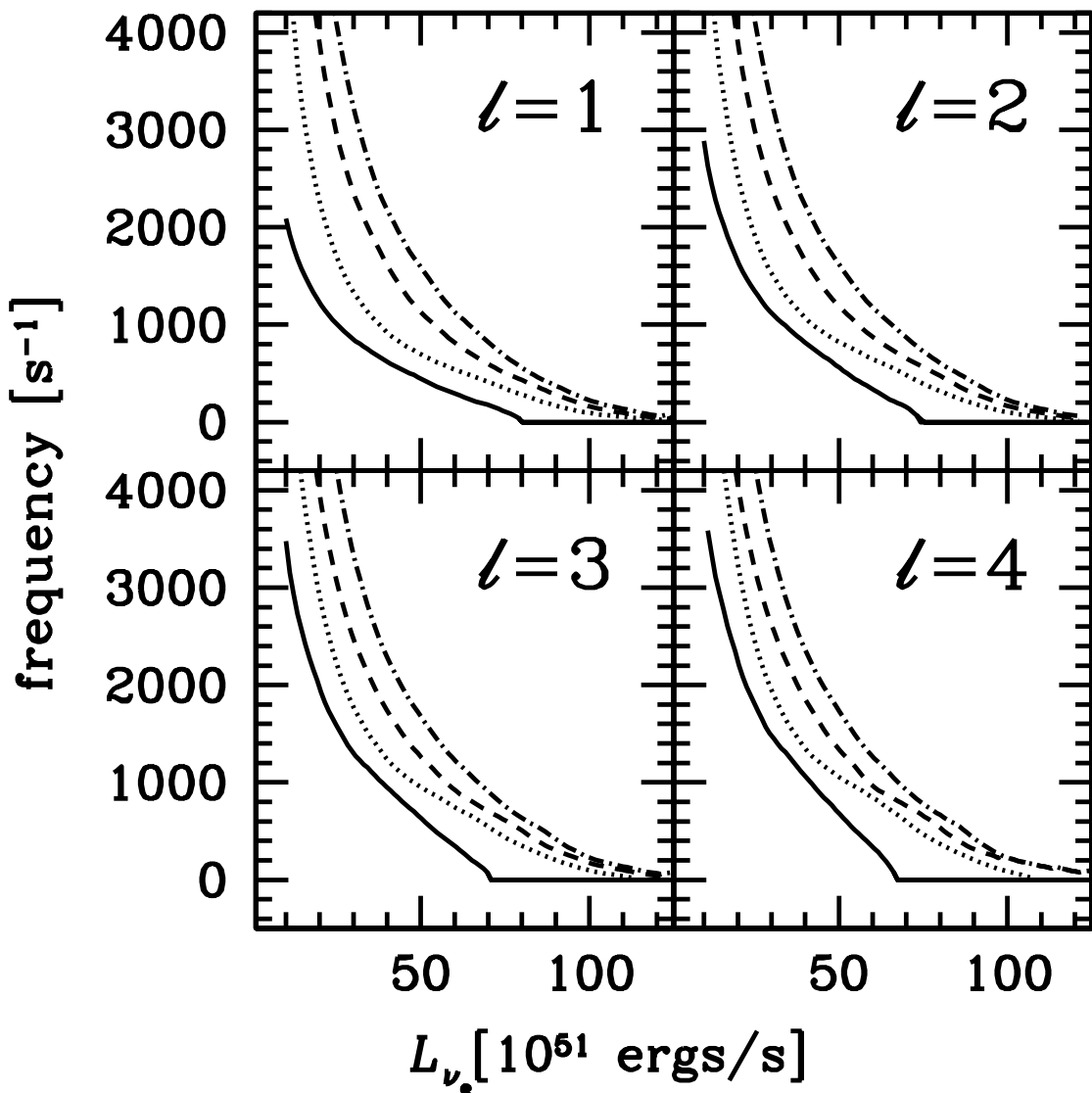


Fig. 3.— The oscillation frequencies, $\text{Im}(\omega)$, the non-radial modes of $l = 1, 2, 3, 4$ as a function of neutrino luminosity. The solid curves represent the fundamental modes while the dotted, dashed and dash-dotted curves correspond to the first, second and third overtones, respectively.

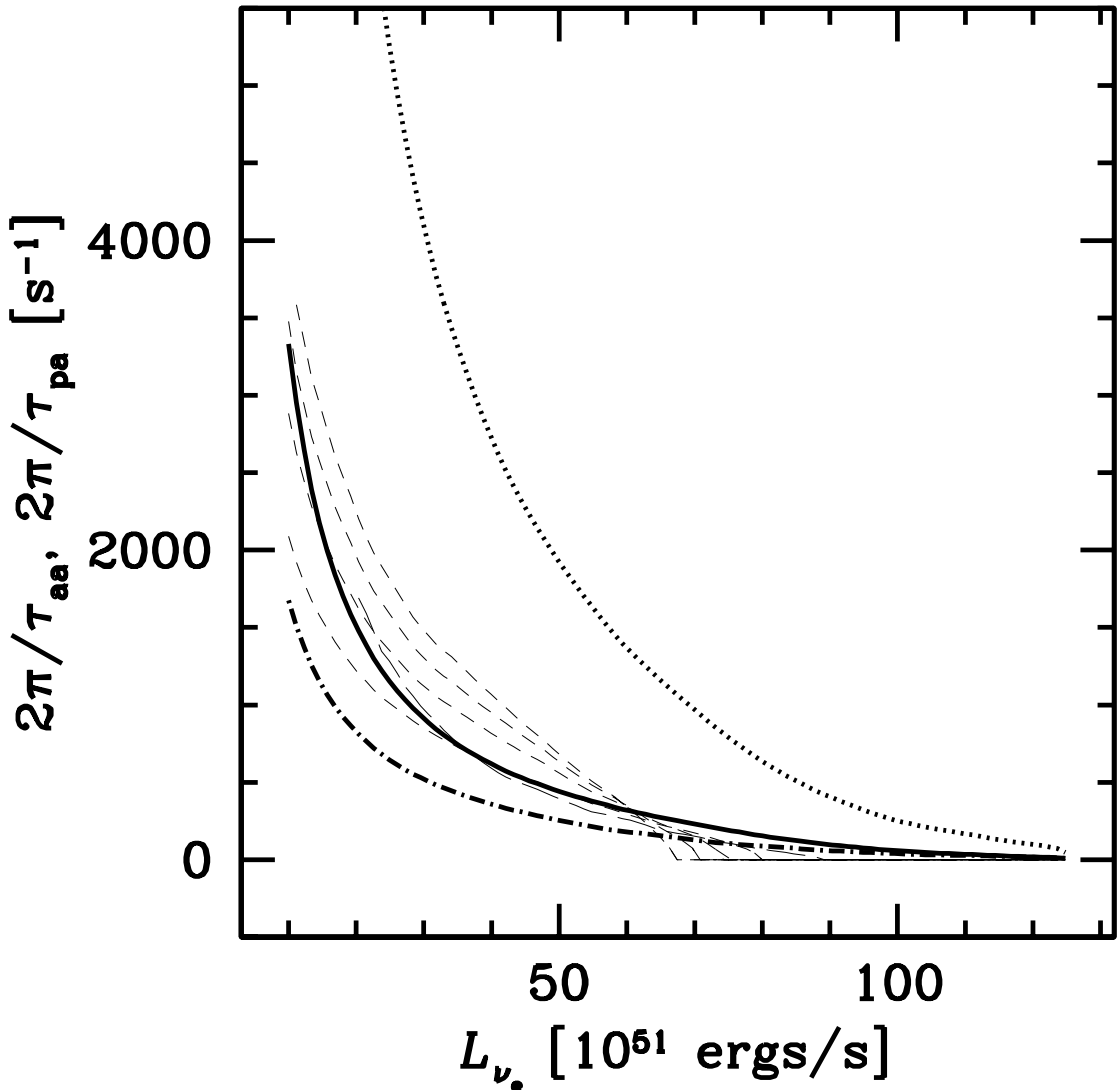


Fig. 4.— The characteristic frequencies of the advection-acoustic cycle, $2\pi/\tau_{\text{aa}}$, and purely acoustic cycle, $2\pi/\tau_{\text{pa}}$, together with the oscillation frequencies for some modes. The solid curve shows $2\pi/\tau_{\text{aa}}$ while the dotted curve gives $2\pi/\tau_{\text{pa}}$. The thin dashed curves represent the oscillation frequencies for the radial (long dashed curve) and non-radial fundamental

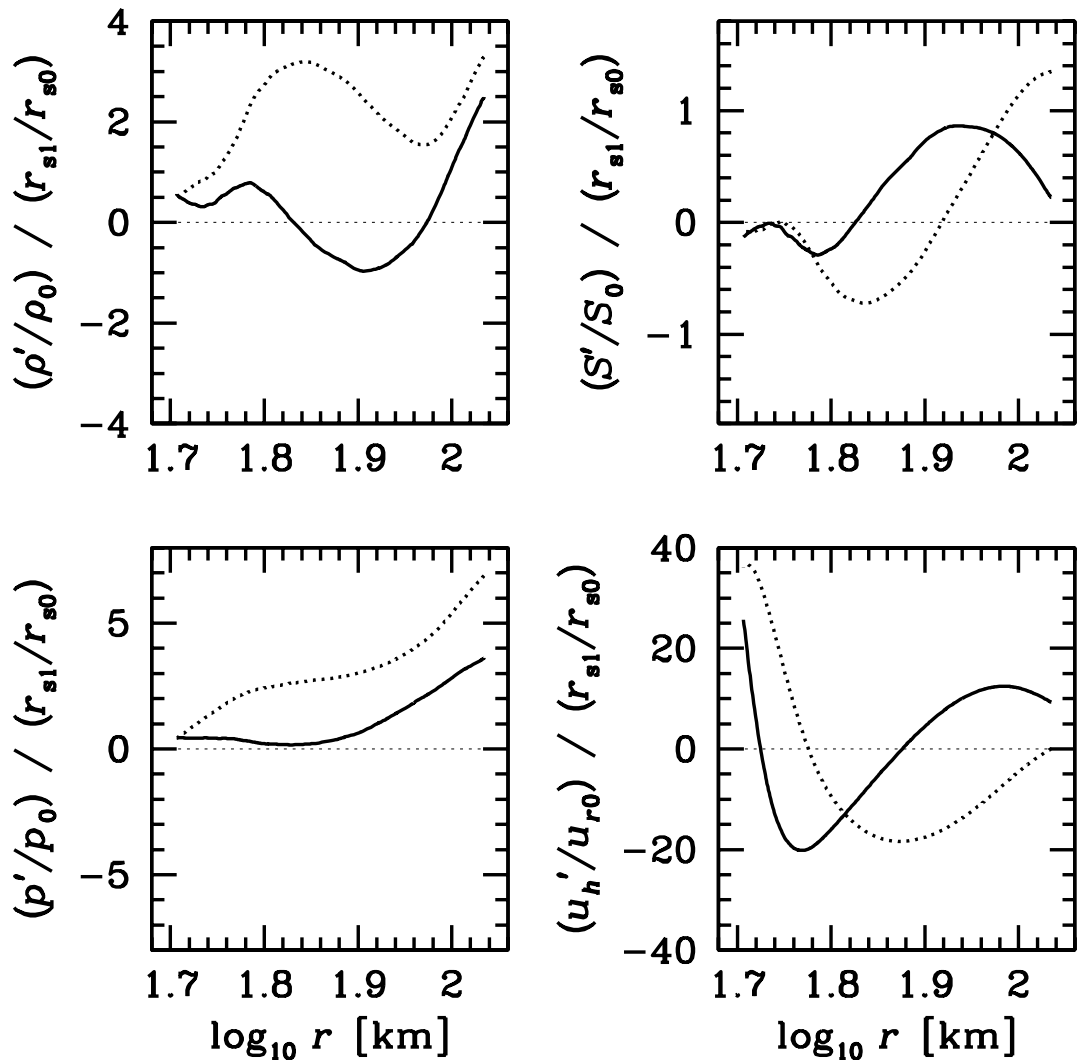


Fig. 5.— The eigen functions of the non-radial unstable mode with $\ell = 1$ for $L_{\nu_e} = 6 \cdot 10^{52}$ ergs/s. The fundamental mode is shown. The solid and dotted curves represent the real and imaginary parts, respectively.

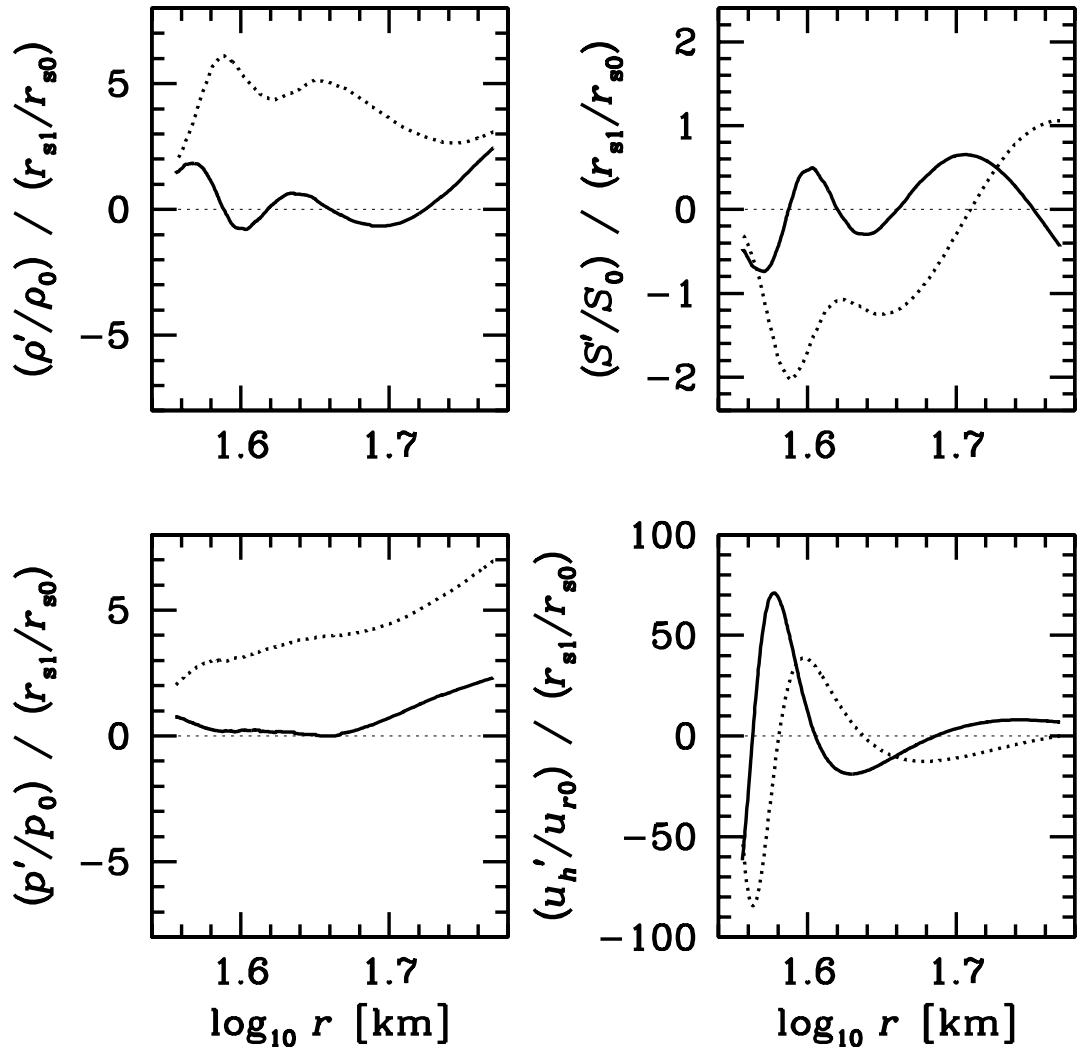


Fig. 6.— The eigen functions of the non-radial unstable mode with $\ell = 2$ for $L_{\nu_e} = 3 \cdot 10^{52}$ ergs/s. The first overtone is shown. The solid and dotted curves represent the real and imaginary parts, respectively.

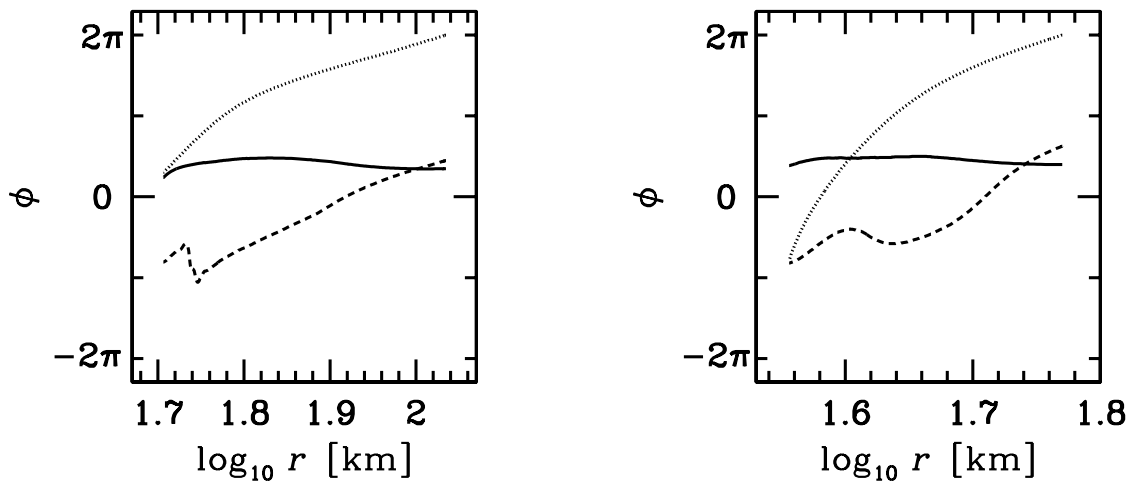


Fig. 7.— (a) The radial profiles of the phases of various perturbed quantities for the fundamental mode of $\ell = 1$ at $L_{\nu_e} = 6 \cdot 10^{52}$ ergs/s. The solid, dotted and dashed curves represent the phases of pressure, horizontal velocity and entropy perturbations, respectively. (b) The same as (a) but for the first overtone of $\ell = 2$ at $L_{\nu_e} = 3 \cdot 10^{52}$ ergs/s.

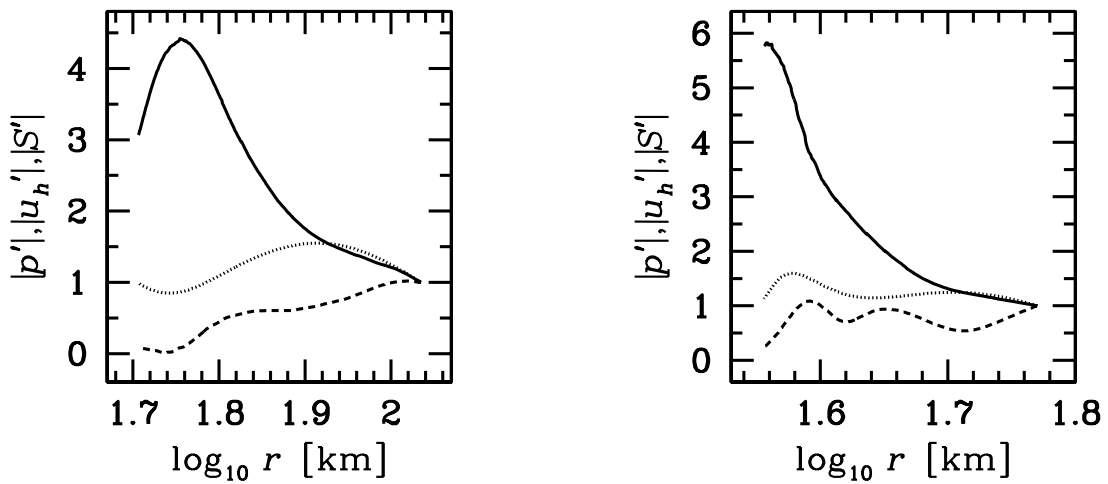


Fig. 8.— (a) The radial profiles of the amplitudes of various perturbed quantities for fundamental mode of $\ell = 1$ at $L_{\nu_e} = 6 \cdot 10^{52}$ ergs/s. The notation is the same as in Fig. 7. The amplitudes are normalized at the shock front. (b) The same as (a) but for the first overtone of $\ell = 2$ at $L_{\nu_e} = 3 \cdot 10^{52}$ ergs/s.

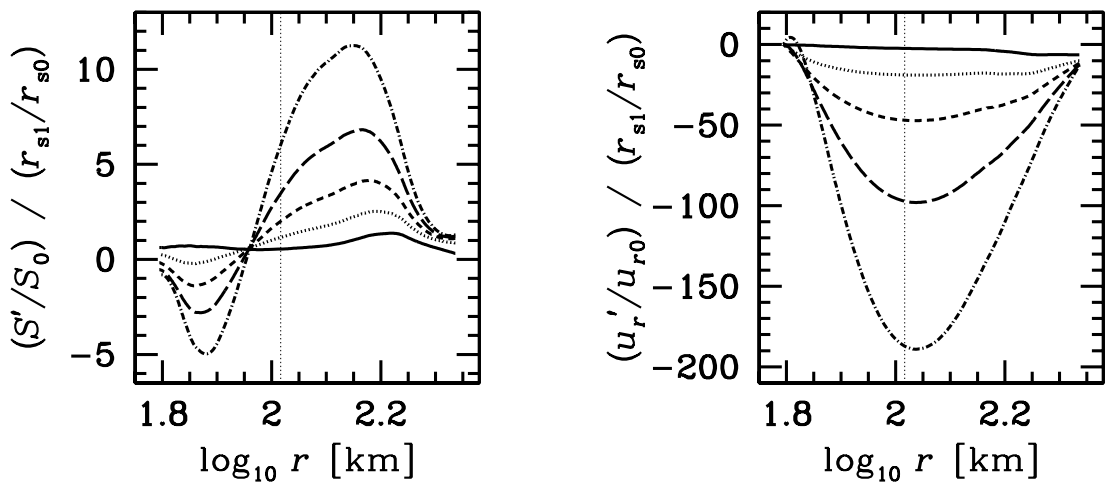


Fig. 9.— (a) The eigen functions of the entropy perturbation for non-oscillatory modes at $L_{\nu_e} = 9 \cdot 10^{52}$ ergs/s. The solid curve represents the radial model ($\ell = 0$). The dotted, dashed, long dashed and dash-dotted curves correspond to the non-radial modes with $\ell = 1, 2, 3, 4$, respectively. Thin dotted line indicates the location of the gain radius. (b) The same as (a) but for the perturbation of radial velocity.

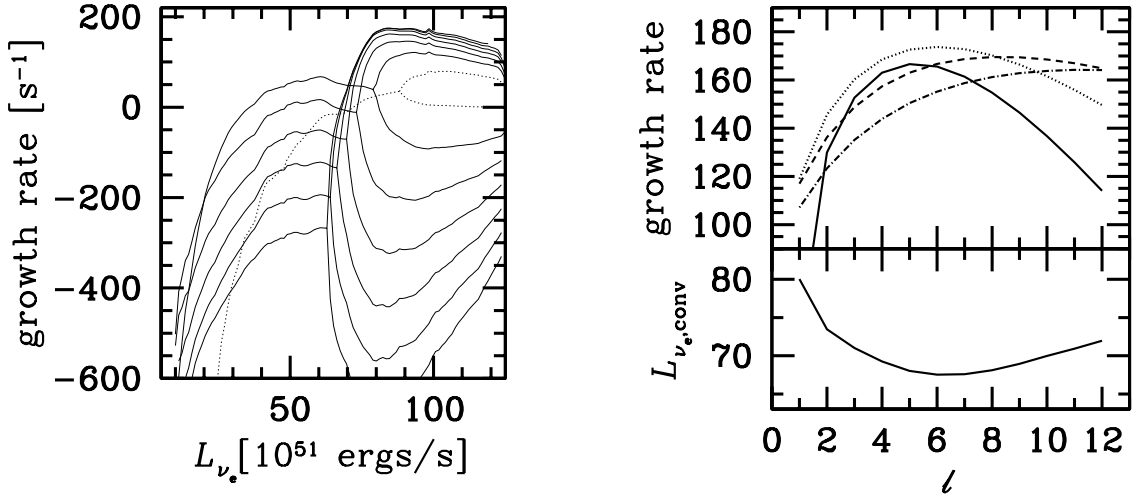


Fig. 10.— (a) The growth rates, $\text{Re}(\omega)$, of the fundamental modes with different ℓ 's. The solid curves represent the non-radial modes with $\ell = 1 - 6$ from top to bottom at $L_{\nu_e} = 5 \cdot 10^{52}$ ergs/s. The dotted curve shows the radial mode ($\ell = 0$). (b) The growth rates, $\text{Re}(\omega)$, of the unstable non-oscillatory modes (the upper branches of the bifurcated modes in (a)) as a function of ℓ . The solid, dotted, dashed and dash-dotted curve correspond to the results for $L_{\nu_e} = 8, 9, 10, 11 \cdot 10^{52}$ ergs/s, respectively. (c) The neutrino luminosity in unit of 10^{51} ergs/s, at which the convective mode with a given ℓ becomes unstable for the first time.

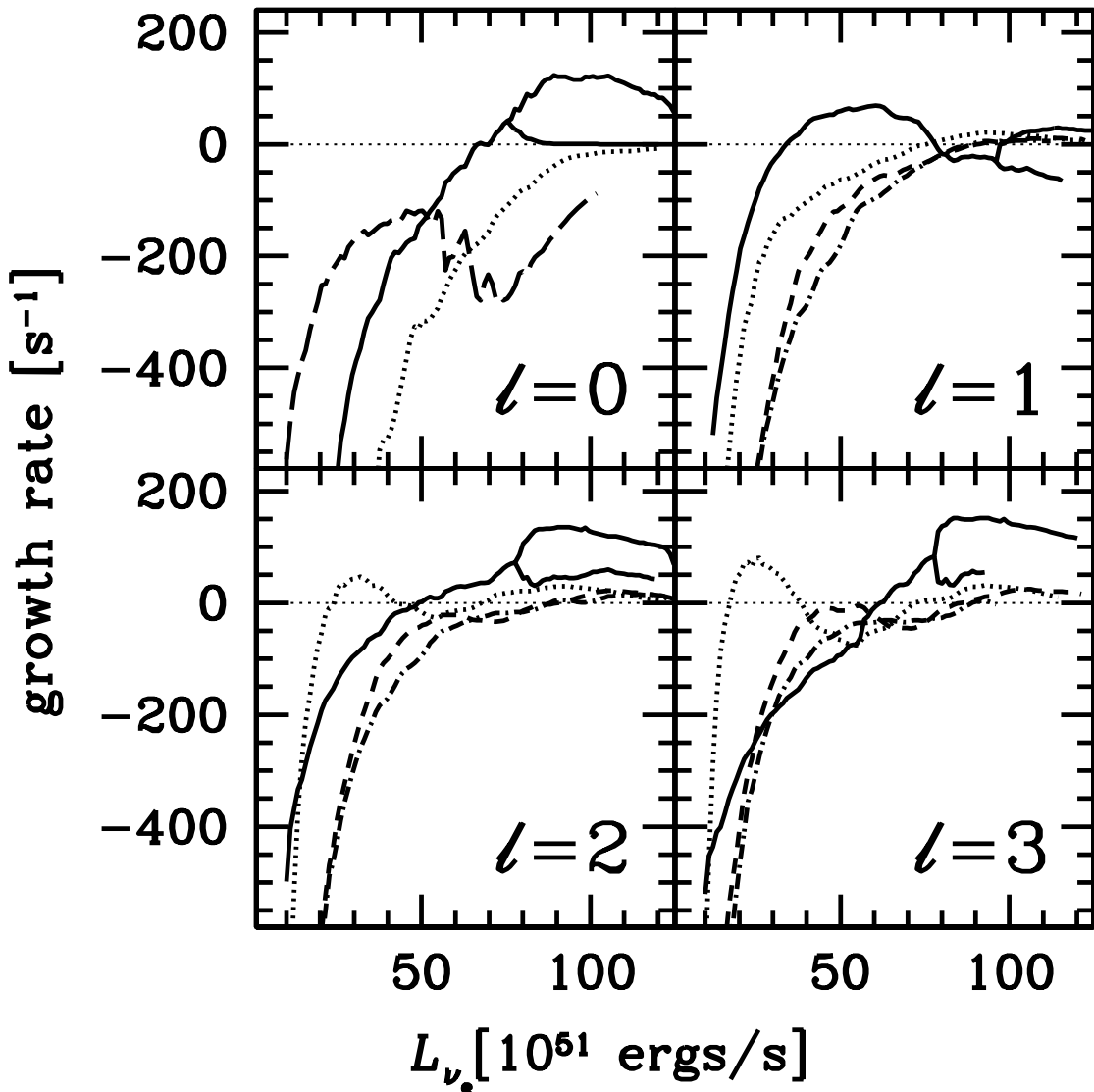


Fig. 11.— The growth rates, $\text{Re}(\omega)$, for the radial, $\ell = 0$, and non-radial modes, $\ell = 1, 2, 3$, as a function of neutrino luminosity. The perturbation of neutrino temperature is taken into account. In the upper left panel, the solid curve represents the fundamental mode and the dotted curve presents the first overtone. The long dashed curve corresponds to the thermal

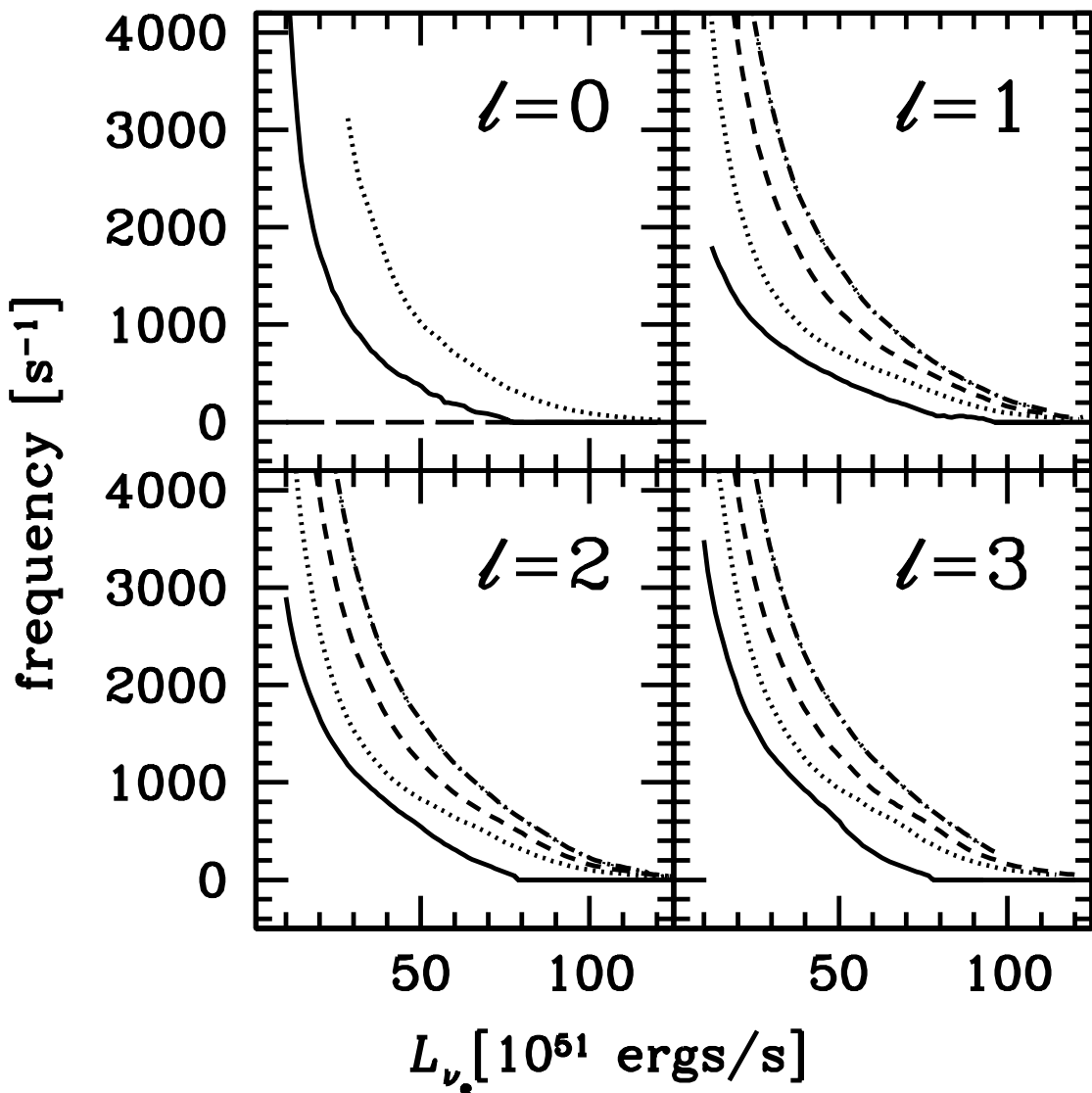


Fig. 12.— The oscillation frequencies, $\text{Im}(\omega)$, for the radial, $\ell = 0$, and non-radial modes, $\ell = 1, 2, 3$, as a function of neutrino luminosity. The perturbation of neutrino temperature is taken into account. In the upper left panel, the solid curve represents the fundamental mode and the dotted curve presents the first overtone. The long dashed curve corresponds

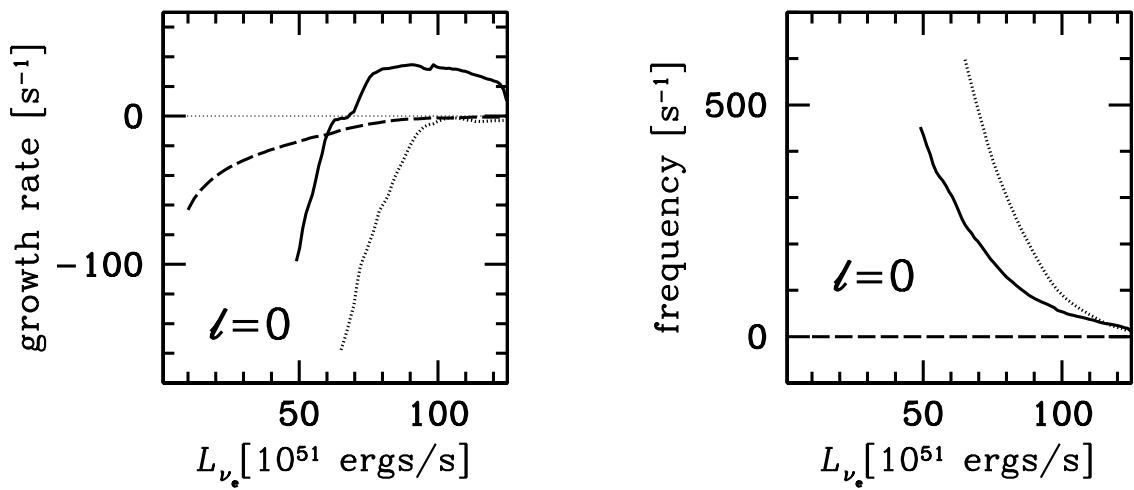


Fig. 13.— (a) The growth rates, $\text{Re}(\omega)$, and (b) oscillation frequencies, $\text{Im}(\omega)$, for representative radial ($\ell = 0$) modes as a function of neutrino luminosity. The perturbations of neutrino temperature and neutrino sphere are taken into account. The long dashed curve denotes the fundamental thermal mode. The solid and dotted curves correspond to the fundamental and first overtone oscillatory modes, respectively.

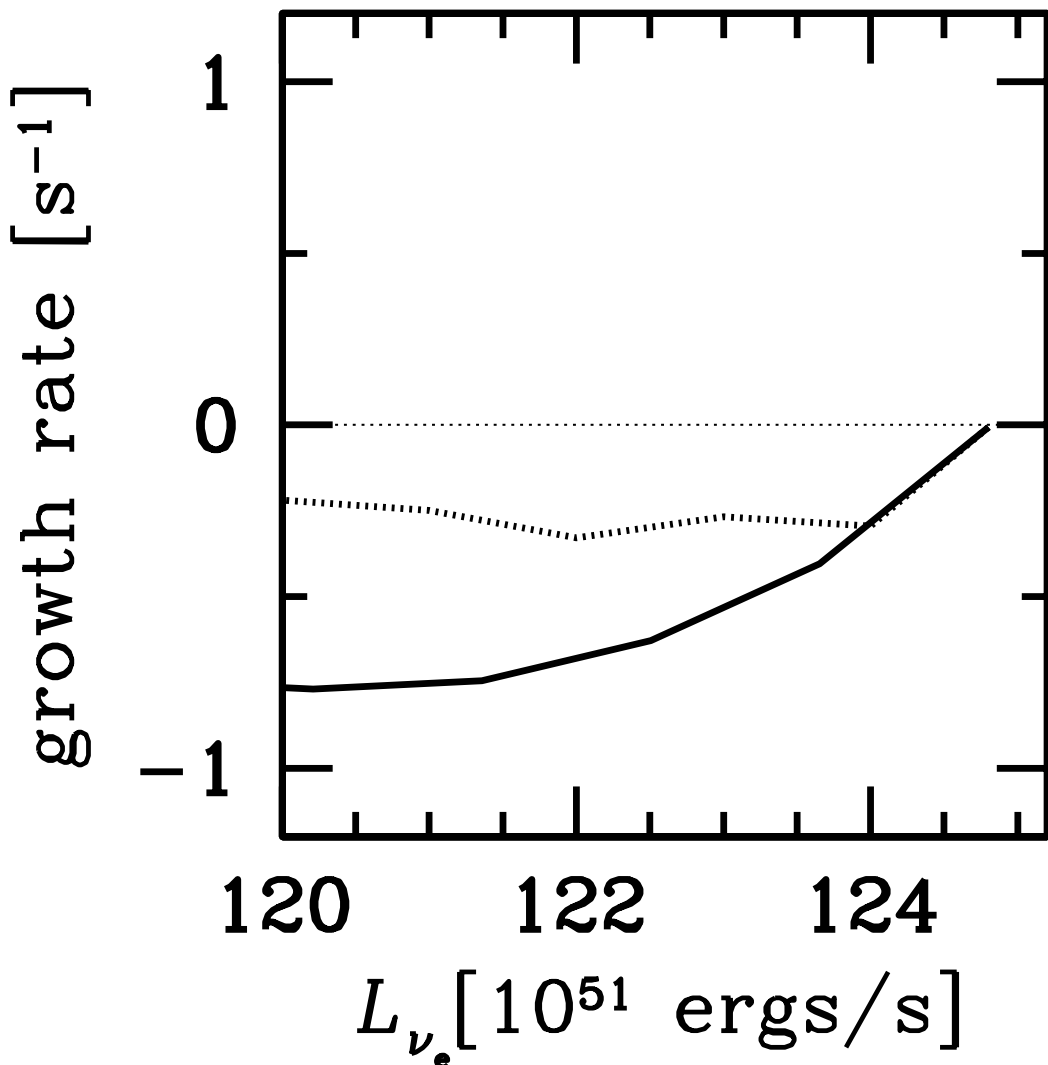


Fig. 14.— The growth rates, $\text{Re}(\omega)$, for the radial ($\ell = 0$) thermal modes as a function of neutrino luminosity. Both the inner solution (solid curve) and the outer solution (dotted curve) are shown. The perturbations of neutrino temperature and neutrino sphere are taken into account.

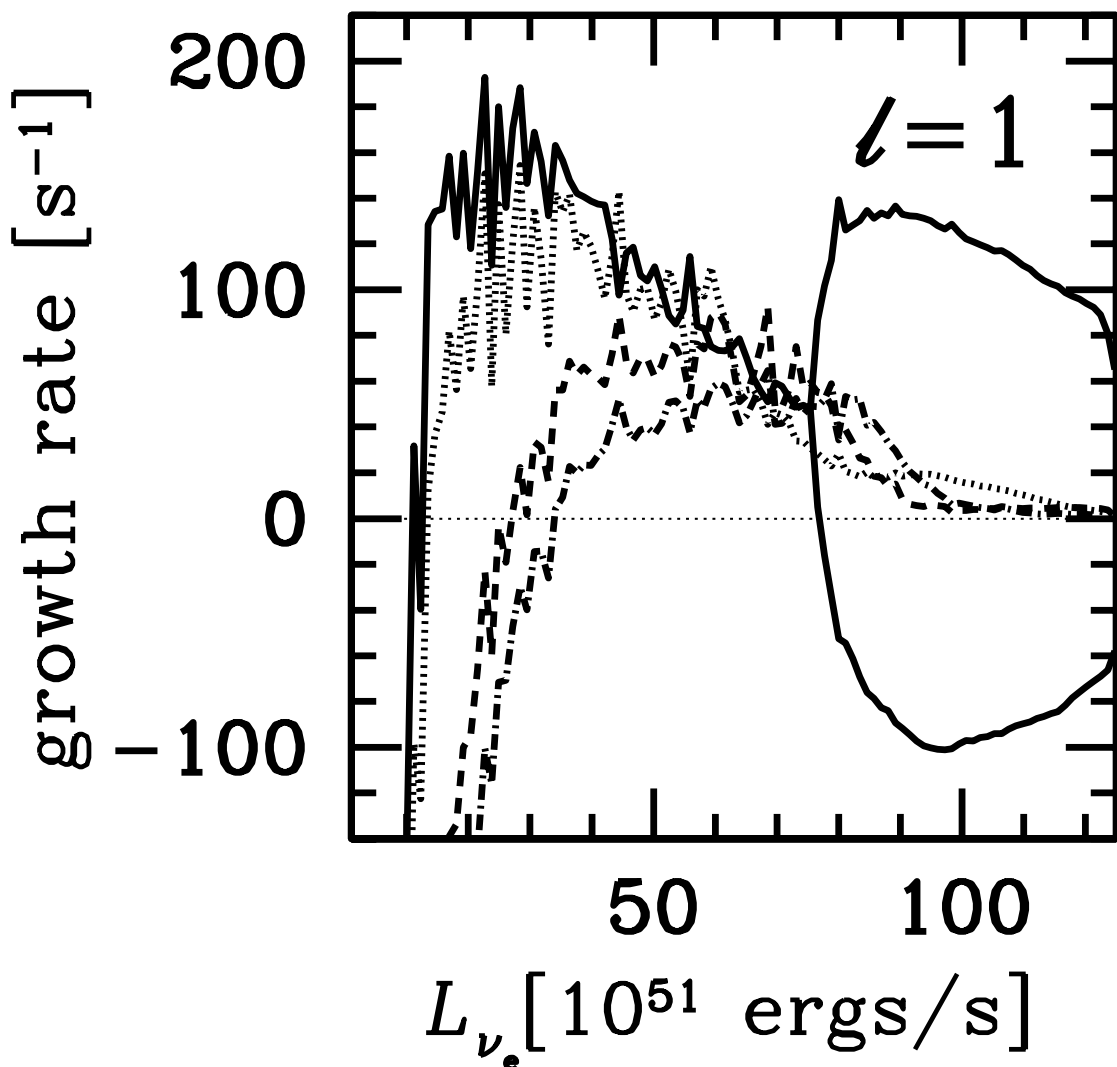


Fig. 15.— The growth rates, $\text{Re}(\omega)$, for $\ell = 1$ modes as a function of neutrino luminosity. The "free" inner boundary condition was imposed for the radial-velocity perturbation. The solid curve represents the fundamental mode while the dotted, dashed and dash-dotted curves correspond to the first, second and third overtones, respectively.